

Fragmentation of positively charged metal clusters in stabilized jellium model with self-compression ^{*}

M. Payami

*Center for Theoretical Physics and Mathematics, Atomic Energy Organization of Iran,
P. O. Box 11365-8486, Tehran, Iran*

(February 5, 2022)

Using the stabilized jellium model with self-compression, we have calculated the dissociation energies and the barrier heights for the binary fragmentation of charged silver clusters. At each step of calculations, we have used the relaxed-state sizes and energies of the clusters. The results for the doubly charged Ag clusters predict a critical size, at which evaporation dominates the fission, in good agreement with the experiment. Comparing the dissociation energies and the fission barrier heights with the experimental ones, we conclude that in the experiments the fragmentation occurs before the full structural relaxation expected after the ionization of the cluster. In the decays of Ag_N^{4+} clusters, the results predict that the charge-symmetric fission processes are dominant for smaller clusters, and the charge-asymmetric fission processes become dominant for sufficiently larger clusters.

^{*}This work is dedicated to the memory of my mother, Gohar and the 68th birthday of my father, Bahram.

I. INTRODUCTION

The fragmentation of ionic metal clusters^{1,2} as well as other properties of metallic clusters have been extensively studied using the jellium model (JM).³⁻⁵ In this model, the discrete ions are replaced by a uniform positive charge background of density $n = 3/4\pi r_s^3$ in which r_s is the bulk value of the Wigner-Seitz (WS) radius of the valence electrons of the metal. The simplest geometry for the positive background is spherical which is appropriate for closed-shell clusters or large enough clusters in which the Jahn-Teller⁶ deformation has negligible contribution. However, using this simple spherical JM, a lot of information on the properties of metal clusters has been obtained. A refined version of the JM, the stabilized^{7,8} jellium model (SJM), which was introduced by Perdew *et al.* in 1990, has improved some drawbacks^{9,10} of the JM (For a recent review on SJM, see Ref.[13]). In recent years, the SJM has been used to predict the properties of bulk metals^{7,11}, metal surfaces¹²⁻¹⁴, metal clusters¹⁵⁻¹⁷ and metallic voids.¹⁸ The fragmentation of charged metal clusters has been also studied^{19,20} by Vieira *et al.* using the SJM. However, since the surface effects have a large contribution in the energetics and sizes of small clusters, and also since in a fission process the competition between the surface tension and coulomb repulsion leads to the existence of a barrier, a more sophisticated use^{15,17} of the SJM is needed to predict the correct energetics of the clusters and the barrier heights (BH) in the study of the fragmentation processes. This method, which is called SJM with self-compression (SJM-SC), has been used to predict the equilibrium sizes and energies of charged²¹ or spin-polarized¹⁷ metal clusters as well as the calculation of chemical potentials of metallic clusters.²² The SJM-SC has been also used by Sarria *et al.*¹⁴ to calculate the surface energies and the work functions of metals. In contrast to the JM and the SJM in which the r_s value is borrowed from the bulk system, in the SJM-SC, the density parameter r_s of the jellium sphere is assumed to be a free parameter which can be adjusted in such a way that a cluster with a given number of electrons and specific electronic configuration achieves its equilibrium state. The SJM-SC calculations on neutral metal clusters^{15,17} has shown that the equilibrium r_s value of the jellium sphere is less than the bulk value and tends to its bulk value for infinitely large cluster. This phenomenon is called self-compression which is due to the dominant effect of surface tension in small metal clusters. However, it has been shown that²¹ charging a small metal cluster can result in an equilibrium r_s value which is larger than the bulk value. This effect is called self-expansion. The self-expansion has been also predicted for highly polarized metal clusters^{17,23}. These two effects have different origins. In the former, the repulsive coulomb force dominates the surface tension whereas, in the latter, the Pauli force is responsible for the self-expansion.

In this work, using SJM-SC, we have studied the binary decay processes of positively charged Ag clusters containing up to 100 atoms in all possible channels. We have considered the following possible decay processes for singly ionized Ag clusters

$$\text{Ag}_N^{1+} \rightarrow \text{Ag}_{N-p}^{1+} + \text{Ag}_p^0, \quad p = 1, 2, \dots, N-2. \quad (1)$$

For doubly charged clusters, the decays can proceed via two different processes. The first one is the evaporation process

$$\text{Ag}_N^{2+} \rightarrow \text{Ag}_{N-p}^{2+} + \text{Ag}_p^0, \quad p = 1, 2, \dots, N-3 \quad (2)$$

and the second one is fission into two charged products

$$\text{Ag}_N^{2+} \rightarrow \text{Ag}_{N-p}^{1+} + \text{Ag}_p^{1+}, \quad p = 2, 3, \dots, [N/2] \quad (3)$$

In general, for the binary decay of Z -ply charged (Z is a positive integer) cluster, we have

$$\text{Ag}_N^Z \rightarrow \text{Ag}_{N-p}^{Z-z_1} + \text{Ag}_p^{z_1}, \quad z_1 = 0, 1, \dots, [Z/2]; \quad p = z_1 + 1, \dots, N - Z + z_1 - 1. \quad (4)$$

For an even value of Z with $z_1 = Z/2$, the range of p reduces to $p = z_1 + 1, \dots, [N/2]$. The processes for which $z_1 = 0$ (i.e., one of the fragments is neutral), are called evaporation processes and others (both fragments are charged) are fission processes. In evaporation processes, the negativity of the difference between total energies before and after fragmentation is sufficient to have a spontaneous decay. However, in fission processes a negative value for the difference energy is not sufficient for the fission of the parent cluster. This is because, the competition between the short-range surface tension and the long-range repulsive coulomb force may give rise to a fission barrier (i.e., one should supply energy to overcome the barrier).

The organization of this paper is as follows. In section II we explain the method of calculating the total energies and fission barriers. To obtain the total energy of a given cluster, we solve the self-consistent Kohn-Sham (KS) equations²⁴ in the density functional theory²⁵ (DFT) with local spin density approximation (LSDA) for the exchange-correlation (XC) functional. To calculate the fission barrier, we use the two-touching-spheres model for the saddle configuration.¹ In section III, we discuss the results, and finally, we conclude this work in section IV.

II. CALCULATIONAL SCHEME

A. Total energy of a cluster

In the context of the SJM, the average energy per valence electron in the bulk with density parameter r_s and polarization ζ is given by²⁶

$$\varepsilon(r_s, \zeta, r_c) = t_s(r_s, \zeta) + \varepsilon_{xc}(r_s, \zeta) + \bar{w}_R(r_s, r_c) + \varepsilon_M(r_s), \quad (5)$$

where

$$t_s(r_s, \zeta) = \frac{c_k}{r_s^2} \left[(1 + \zeta)^{5/3} + (1 - \zeta)^{5/3} \right] \quad (6)$$

$$\varepsilon_{xc}(r_s, \zeta) = \frac{c_x}{r_s} \left[(1 + \zeta)^{4/3} + (1 - \zeta)^{4/3} \right] + \varepsilon_c(r_s, \zeta) \quad (7)$$

$$c_k = \frac{3}{10} \left(\frac{9\pi}{4} \right)^{2/3}; \quad c_x = \frac{3}{4} \left(\frac{9}{4\pi^2} \right)^{1/3}. \quad (8)$$

All equations throughout this paper are expressed in Rydberg atomic units. Here t_s and ε_{xc} are the mean noninteracting kinetic energy and the exchange-correlation energy per particle, respectively. For ε_c we use the Perdew-Wang parametrization.²⁷ For a z -valent metal the average Madelung energy, ε_M , is defined as $\varepsilon_M = -9z/5r_0$, in which r_0 is the radius of the WS sphere, $r_0 = z^{1/3}r_s$. In Eq.(5), $\zeta = (n_\uparrow - n_\downarrow)/(n_\uparrow + n_\downarrow)$ in which n_\uparrow and n_\downarrow are the spin densities of the homogeneous system with total density $n = n_\uparrow + n_\downarrow$. The quantity \bar{w}_R is the average value (over the WS cell) of the repulsive part of the Ashcroft empty core²⁸ pseudopotential,

$$w(r) = -\frac{2z}{r} + w_R, \quad w_R = +\frac{2z}{r}\theta(r_c - r), \quad (9)$$

and is given by $\bar{w}_R = 3r_c^2/r_s^3$ where, z is the valence of the atom, $\theta(x)$ is the ordinary step function which assumes the value of unity for positive arguments, and zero for negative values.

The core radius is fixed to the bulk value, r_c^B , by setting the pressure of the unpolarized bulk system equal to zero at the observed equilibrium density $\bar{n} = 3/4\pi[\bar{r}_s^B(0)]^3$:

$$\left. \frac{\partial}{\partial r_s} \varepsilon(r_s, 0, r_c) \right|_{r_s=\bar{r}_s^B(0), r_c=r_c^B} = 0. \quad (10)$$

Here, $\bar{r}_s^B(0) \equiv \bar{r}_s^B(\zeta = 0)$ is the observed equilibrium density parameter for the unpolarized bulk system, and takes the value of 3.02 for Ag. The derivative is taken at fixed r_c , and the solution of the above equation gives r_c^B as a function of $\bar{r}_s^B(0)$

$$r_c^B[\bar{r}_s^B(0)] = \frac{1}{3}[\bar{r}_s^B(0)]^{3/2} \left\{ \left[-2t_s(r_s, 0) - \varepsilon_x(r_s, 0) + r_s \frac{\partial}{\partial r_s} \varepsilon_c(r_s, 0) - \varepsilon_M(r_s) \right]_{r_s=\bar{r}_s^B(0)} \right\}^{1/2}. \quad (11)$$

The SJM energy for a spin-polarized system with boundary surface is given by⁷

$$\begin{aligned} E_{\text{SJM}}[n_\uparrow, n_\downarrow, n_+] &= E_{\text{JM}}[n_\uparrow, n_\downarrow, n_+] + (\varepsilon_M(r_s) + \bar{w}_R(r_s, r_c^B)) \int d\mathbf{r} n_+(\mathbf{r}) \\ &\quad + \langle \delta v \rangle_{\text{WS}}(r_s, r_c^B) \int d\mathbf{r} \Theta(\mathbf{r}) [n(\mathbf{r}) - n_+(\mathbf{r})], \end{aligned} \quad (12)$$

where

$$\begin{aligned} E_{\text{JM}}[n_\uparrow, n_\downarrow, n_+] &= T_s[n_\uparrow, n_\downarrow] + E_{xc}[n_\uparrow, n_\downarrow] \\ &\quad + \frac{1}{2} \int d\mathbf{r} \phi([n, n_+]; \mathbf{r}) [n(\mathbf{r}) - n_+(\mathbf{r})] \end{aligned} \quad (13)$$

and

$$\phi([n, n_+]; \mathbf{r}) = 2 \int d\mathbf{r}' \frac{[n(\mathbf{r}') - n_+(\mathbf{r}')] }{|\mathbf{r} - \mathbf{r}'|}. \quad (14)$$

Here, $n = n_\uparrow + n_\downarrow$ and n_+ is the jellium density. $\Theta(\mathbf{r})$ takes the value of unity inside the jellium background and zero, outside. The first and second terms in the right hand side of Eq.(13) are the non-interacting kinetic energy and the exchange-correlation energy, and the last term is the Coulomb interaction energy of the system. The quantity $\langle \delta v \rangle_{\text{WS}}$ is the average of the difference potential over the Wigner-Seitz cell and the difference potential, δv , is defined as the difference between the pseudopotential of a lattice of ions and the electrostatic potential of the jellium positive background. The effective potential, used in the self-consistent KS equations, is obtained by taking the variational derivative of the SJM energy functional with respect to the spin densities as

$$\begin{aligned} v_{eff}^\sigma([n_\uparrow, n_\downarrow, n_+]; \mathbf{r}) &= \frac{\delta}{\delta n_\sigma(\mathbf{r})} (E_{\text{SJM}} - T_s) \\ &= \phi([n, n_+]; \mathbf{r}) + v_{xc}^\sigma([n_\uparrow, n_\downarrow]; \mathbf{r}) + \Theta(\mathbf{r}) \langle \delta v \rangle_{\text{WS}}(r_s, r_c^B), \end{aligned} \quad (15)$$

where $\sigma = \uparrow, \downarrow$. By solving the KS equations

$$(\nabla^2 + v_{eff}^\sigma(\mathbf{r})) \phi_i^\sigma(\mathbf{r}) = \varepsilon_i^\sigma \phi_i^\sigma(\mathbf{r}), \quad \sigma = \uparrow, \downarrow, \quad (16)$$

$$n(\mathbf{r}) = \sum_{\sigma=\uparrow, \downarrow} n_\sigma(\mathbf{r}), \quad (17)$$

$$n_\sigma(\mathbf{r}) = \sum_{i(\text{occ})} |\phi_i^\sigma(\mathbf{r})|^2, \quad (18)$$

and finding the self-consistent values for ε_i^σ and ϕ_i^σ , one obtains the total energy.

In our spherical JM, we have

$$n_+(\mathbf{r}) = \frac{3}{4\pi r_s^3} \theta(R - r) \quad (19)$$

in which $R = (zN)^{1/3} r_s$ is the radius of the jellium sphere, and $n(\mathbf{r})$ denotes the electron density at point \mathbf{r} in space. Using the Eq. (21) of Ref. [7], this average value is given by

$$\langle \delta v \rangle_{\text{WS}}(r_s, r_c^B) = \frac{3(r_c^B)^2}{r_s^3} - \frac{3}{5r_s}. \quad (20)$$

Applying Eq. (12) to a metal cluster which contains N_\uparrow spin-up, N_\downarrow spin-down and $N (= N_\uparrow + N_\downarrow)$ total electrons in the ground state, the SJM energy becomes a function of N , r_s , and r_c^B . The equilibrium density parameter, $\bar{r}_s(N)$, for a cluster in the ground state electronic configuration, is the solution of the equation

$$\left. \frac{\partial}{\partial r_s} E(N, r_s, r_c^B) \right|_{r_s = \bar{r}_s(N)} = 0. \quad (21)$$

Here, the derivative is taken at fixed values of N and r_c^B . For an N -electron cluster in its ground state electronic configuration, we have solved the KS equations²⁴ self-consistently for various r_s values and obtained the equilibrium density parameter, $\bar{r}_s(N)$, and its corresponding energy, $\bar{E}(N) \equiv E(N, \bar{r}_s(N), r_c^B)$.

B. Dissociation energy and fission barrier

The dissociation energy (DE) for the general binary decay process (4), defined as the difference in the sum of total energies of the products and the total energy of the parent cluster, is given by

$$D_{z_1}^Z(N, p) = (E_{N-p}^{Z-z_1} + E_p^{z_1}) - E_N^Z, \quad (22)$$

In evaporation processes ($z_1 = 0$), a negative value for the DE implies that the parent cluster is unstable against that particular decay channel and therefore, the fragmentation is spontaneous. On the other hand, a positive DE in a particular decay channel means that the parent cluster is stable against the decay in that particular channel. That is, one should somehow supply energy to the system to induce the fragmentation. For processes (1) and (2) the DE becomes

$$D_0^{1+}(N, p) = (E_{N-p}^{1+} + E_p^0) - E_N^{1+} \quad (23)$$

and

$$D_0^{2+}(N, p) = (E_{N-p}^{2+} + E_p^0) - E_N^{2+}, \quad (24)$$

respectively. However, in the fission processes ($z_1 > 0$) as in Eq.(3), a negative DE does not mean that the cluster would decay. It is because of the existence of a fission barrier which originates from the short-range attractive (due to binding energy) and long-range repulsive (due to coulomb repulsion) forces between the charged products. The situation is shown in Fig. 1. Any excitation above the barrier, which may be induced by collisions or radiation, will eventually make the expected decay possible. One of the main deficiencies of the JM is that it gives negative values⁹ of surface energies for $r_s \leq 2$. Our using of SJM-SC is expected, therefore, to give more realistic values of surface energies and barrier heights. The fission barrier $B_{z_1}^Z(N, p)$ is approximated by the Coulomb interaction E_c of two touching spheres (i.e., the fission products) and the DE as

$$B_{z_1}^Z(N, p) = D_{z_1}^Z(N, p) + E_c \quad (25)$$

For the Coulomb interaction between the two fission products we take into account their polarizabilities. The interaction energy of two charged conducting spheres can be calculated numerically using image charge method.¹ An equally good but much simpler approach is the use of the analytical expression^{29,30} for the interaction between charges z_1 and z_2 with polarizabilities α_1 and α_2 at a distance s

$$E_{1,2}^{\text{pol}}(s) = \frac{A_2}{A_4} \frac{2z_1 z_2}{s} - \frac{\alpha_1}{s^3} \frac{1}{A_4} \frac{z_2^2}{s} - \frac{\alpha_2}{s^3} \frac{1}{A_4} \frac{z_1^2}{s}. \quad (26)$$

Here A_j is given by

$$A_j = 1 - \frac{j\alpha_1\alpha_2}{s^6}, \quad (27)$$

and the polarizability of a conducting sphere (i.e., the metal cluster) with radius R is³¹ $\alpha = R^3$. An other formula which was used^{1,32} for the Coulomb interaction of two touching conducting spheres is given by

$$E_{1,2} = \frac{2z_1 z_2}{R_1 + R_2 + 2\delta R} \quad (28)$$

where, for silver, the value $\delta R = 0.94$ takes the polarizability into account. The BH's for small clusters, obtained from this formula, are somewhat smaller than those we obtained using Eqs. (26), (27). Koizumi *et. al.*^{33,34} have calculated the barrier heights for the fission of doubly charged silver clusters using a shape function in the LDM with shell correction.

III. RESULTS AND DISCUSSION

After an extensive self-consistent SJM-SC calculations, we have calculated the equilibrium r_s values and the energies of Ag_N^Z ($Z=0,1,2,3,4$) for different cluster sizes ($1 \leq N \leq 100$). To show the main differences in the equilibrium r_s values of these clusters, which are appreciable for relatively small clusters, we have plotted, in Fig. 2, the corresponding $\bar{r}_s(N)$ values only up to $N = 34$. As is obviously seen in the figure, the neutral and singly ionized clusters are self-compressed for all values of N . This is because of the dominant effect of the surface tension. However, for multiply charged clusters, the $\bar{r}_s(N)$ values cross the bulk border (i.e., $r_s = 3.02$) at some N which we show it by N_0 . Our results show that, in general, for larger values of charging, the self-expansion persists up to larger values of N_0 . That is, $N_0^{2+} < N_0^{3+} < N_0^{4+} < \dots$. For example, here we have obtained the values of 7, 17, 23 for N_0^{2+} , N_0^{3+} , N_0^{4+} , respectively. This means that, for larger charging values, the coulomb repulsion between excess charges dominates

the surface tension up to larger values of N_0 . It is also clearly seen in Fig. 2 that for clusters with the same numbers of electrons but different numbers of atoms, N , the following inequality holds

$$\bar{r}_s^0(N) < \bar{r}_s^{1+}(N+1) < \bar{r}_s^{2+}(N+2) < \bar{r}_s^{3+}(N+3) < \dots \quad (29)$$

For Ag_N^{4+} clusters, we could not find any solution of the Eq. (21) for $N = 5$. That is, the single remaining electron is not able to bind the 5 constituent ions to each other in the Ag_5^{4+} system. However, the solutions of $\bar{r}_s^{4+}(6) = 14.76$ and $\bar{r}_s^{3+}(4) = 29.0$ have been obtained for Eq. (21) which are so large that one can not realize the corresponding bound states experimentally and we ignore these bound states.

Figure 3 shows the equilibrium energies per atom in electron-volts for Ag_N^0 , Ag_N^{1+} , Ag_N^{2+} , Ag_N^{3+} , and Ag_N^{4+} with different cluster sizes ($1 \leq N \leq 34$). For comparison, we have also plotted the bulk value ($\varepsilon = -7.89\text{eV}$) by a dashed line. As is seen, by increasing the charge of a given N -atom cluster, the coulomb repulsion between the excess charge induces an inflation in the cluster (see Fig. 2) and therefore, the density of the material in the cluster decreases which, in turn, leads to a smaller binding energies.

In Fig. 4(a) we have plotted the DE's of the most favored decay channels for the process $\text{Ag}_N^{1+} \rightarrow \text{Ag}_{N-p}^{1+} + \text{Ag}_p^0$. By definition, the DE is minimum in the most favored channel. We have shown the most favored value of p by p^* . The solid small square symbols show the most favored values p^* on the right vertical axis whereas, the corresponding DE's, $D_0^{1+}(N, p^*)$, are shown on the left vertical axis by large open squares. The dashed line is the result of a fitting to the quantal DE's. As is seen, the majority of the clusters have positive DE's and therefore, they are stable against the spontaneous decay. However, the remaining clusters have negative DE's and accordingly, they decay into smaller fragments. Clusters close to the closed-shell ones, decay by emitting a monomer or dimer. On the other hand, clusters that are far from being a closed-shell, can break into two fragments each of which are close or identical to closed-shell ones. For example, Ag_3^{1+} emits a neutral monomer and the remaining is a singly charged dimer, Ag_{44}^{1+} emits an Ag_8^0 which is a closed-shell and the remaining is Ag_{36}^{1+} which is close to a closed-shell, and finally, Ag_{80}^{1+} emits Ag_{20}^0 and the situation is similar to the latter one. Except for the closed-shell singly ionized cluster Ag_{69}^{1+} , all other closed-shell singly ionized clusters, Ag_N^{1+} ($N=3, 9, 19, 21, 35, 41, 59, 91, 93$) are stable against the spontaneous decay. The dashed fitted line which resembles the result of liquid-drop model (LDM) calculations (see Fig. 4 of Ref. [19]), predicts that all singly ionized clusters are stable and the asymptotic value of DE is constant and equal to 0.20eV .

Figure 4(b) compares the experimental³⁵ dissociation energies with the monomer DE's $D_0^{1+}(N, 1)$, dimer DE's $D_0^{1+}(N, 2)$, and the most favored DE's $D_0^{1+}(N, p^*)$. As is seen, the most favored fragments are somewhere monomers, somewhere dimers and somewhere none of them. The general trend of the calculated monomer dissociation energies is similar to the experimental one and has a better agreement with the experiment than the other two DE's. That is, from $N = 3$ to $N = 4$ the energy decreases; from $N = 4$ to $N = 9$ the energy increases in the mean; a decrease on going from 9 to 10; an increase from 10 to 21; and finally, a decrease from $N = 21$ to $N = 22$ and again increasing from $N = 22$. However, our results lack the odd-even staggering because, it originates from the nonspherical shapes for the jellium. Resorting to non-spherical shapes also decreases the pronounced shell effects.³² The relative smallness of our calculated DE's can be explained in terms of the details of the experimental setup. If the experiment starts using neutral Ag_N clusters, then the equilibrium r_s values would be smaller than the bulk value (see the $Z = 0$ plot in Fig. 2), and therefore, the total energies would be more negative (see the $Z = 0$ plot in Fig. 3). Now, irradiating the parent neutral cluster with a high power laser beam would lead to the ionization of the neutral cluster. If the photons also interact with the ionized cluster before the ionized cluster achieves its relaxed state, then the equilibrium r_s value of the ionized cluster would be less than the relaxed value (In our calculations we have used the relaxed values at all steps.), and therefore, the magnitude of the total energy of the ionized parent cluster would be larger. This fact would lead to larger values of the DE's. Comparing the experimental data with our results we conclude that the photo-dissociation occurs before the relaxation of the parent ionized cluster is completed. The other extreme is that we consider the 'sudden' approximation in which we assume that the relaxation time for the ionized cluster is infinite and the cluster undergoes the dissociation without changing the volume (i.e., the saturation approximation which is used in nuclear fragmentations and ordinary jellium calculations for clusters). In reality, neither of these extreme 'relaxed' or 'sudden' approximations are at work but something in between.

In Fig. 5(a) we have shown the most favored products $\text{Ag}_{p^*}^0$ and the dissociation energies $D_0^{2+}(N, p^*)$ for the decay of Ag_N^{2+} via evaporation channel. For this process, as in singly ionized case, the dashed fitted line predicts no spontaneous decays and shows a higher constant asymptotic DE as 0.40eV . The most favored products are mainly monomers, dimers and octamers.

Figure 5(b) shows the barrier heights $B_{1+}^{2+}(N, p^*)$ for the most favored channels of the process $\text{Ag}_N^{2+} \rightarrow \text{Ag}_{N-p}^{1+} + \text{Ag}_p^{1+}$. By definition, the most favored fission channel has a minimum value for the BH. As is seen, some of the BH's are negative. The negativity of a BH means that we need no energy to supply the system to initiate the fission. The dashed line which shows the mean behavior of BH intersects the zero line at $N_a^{\text{mean}} \approx 29$ (the mean appearance size).

This means that on the average, all Ag_N^{2+} clusters with $N < 29$ are unstable against spontaneous fission. The values of p^* show that most of the emitted fragments are closed-shell Ag_N^{1+} clusters with $N = 3, 9, 21$.

In Fig. 5(c) we have compared the most favored decays of Figs. 5(a) and 5(b). It is clearly seen that in a certain size range, the fission and evaporation definitely start their competition. Our quantal results in Fig. 5(c) show that in the size range $21 \leq N \leq 26$ the evaporation dominates the fission which is in good agreement with the Katakuse *et. al.* experimental results³⁶ that reveal fission for $N \leq 22$. However, our result is slightly larger than the Krückeberg *et. al.*³⁰ experimental data which show that the fission occurs for $N \leq 16$. This difference in the experimental results depends on the details of the experiment. For $N > 26$, our results show that fission dominates again. To estimate the size range at which evaporation completely dominates the fission, we simply find the intersection point of the two mean behaviors (dashed lines) in Figs. 5(a) and 5(b). A simple calculation gives this mean critical value as $N_c^{\text{mean}} \approx 50$. That is, in an induced fragmentation experiment of Ag_N^{2+} clusters, the evaporation dominates the fission for $N > 50$.

In Fig. 5(d) we have compared the most favored values $D_0^{2+}(N, p^*)$ and $B_{1+}^{2+}(N, p^*)$ with the experimental threshold energies³⁰. Here, also we have smaller DE's and BH's compared to the experiment. One reason for this behavior is that the equilibrium volume of the parent cluster is not equal to the sum of the equilibrium volumes of the product clusters (i.e., the 'relaxed' approximation) but is larger. The larger value of the equilibrium r_s leads to a smaller magnitude of the initial energy and therefore, by Eq. (25) to a smaller barrier heights. In other words, the energy needed to deform the parent cluster toward the fission (In deformation the surface area increases.) is partly paid as a result of self-expansion of the parent cluster. Our calculations show that in almost all decay channels, the sum of volumes of the decay products is smaller than that of the parent cluster which can be explained by the fact that in smaller clusters the surface effect is higher than that in larger clusters. The calculated results for the most favored values of DE's at $N = 9$ and $N = 10$ are very close to the experimental values. The most favored products at $N = 9$ and $N = 10$ are neutral dimer and monomer, respectively (see Fig. 5(a)).

In Fig. 5(e) we have compared the calculated monomer DE's $D_0^{2+}(N, 1)$ and the singly charged trimer BH's $B_{1+}^{2+}(N, 3)$ with the experiment. Here also the difference is appreciable.

In Fig. 6(a) we have plotted the p^* and the $D_0^{3+}(N, p^*)$ for different cluster sizes. The situation is similar to other previous evaporation processes. Here also the asymptotic behavior of the fitted line predicts no decay and has a constant value of about 0.50eV .

In Fig. 6(b), we have plotted the BH's $B_{1+}^{3+}(N, p^*)$ for the most favored channel of the binary fission of the process $\text{Ag}_N^{3+} \rightarrow \text{Ag}_{N-p}^{2+} + \text{Ag}_p^{1+}$. Here, the fission products with smaller charge are more or less the same as those in the fission of Ag_N^{2+} clusters. The mean behavior dashed line intersects the zero axis at $N_a^{\text{mean}} \approx 53$. The slope of this line is larger than that of Fig. 5(b).

Figure 6(c) compares the most favored decays of Figs. 6(a) and 6(b). To our knowledge, there is no experimental results in the literature on the decay of Ag_N^Z with $Z \geq 3$. It is seen that at $N = 38$, evaporation dominates and from $N = 39$ to $N = 42$ evaporation and fission are equally probable. From $N = 43$ to $N = 58$, except for $N = 54$, fission dominates again. From $N = 59$ to $N = 67$ the evaporation process overcomes and so on. To obtain the mean critical value, we find the intersection point of the two mean behaviors (dashed lines) in Figs. 6(a) and 6(b) which results in the value $N_c^{\text{mean}} \approx 80$.

Fig. 7(a) plots the p^* and the $D_0^{4+}(N, p^*)$ for the evaporation processes of Ag_N^{4+} . In this figure, one notes the unstability of two smallest sized Ag_7^{4+} , Ag_8^{4+} and the stability of almost all others against the evaporation. The fitted dashed line predicts no evaporation and has the asymptotic value of 0.75eV . The evaporation products are seen to be mostly neutral dimers and a few monomers and octamers.

In Fig. 7(b) we have plotted the p^* and the $B_{1+}^{4+}(N, p^*)$ as functions of N . We see that at $N = 21$ the BH becomes positive for the first time. The dashed line shows the mean behavior of the fission barriers. This fitted line has crossed the zero axis at $N_1^{\text{mean}} \approx 74$. That is, on the average, the Ag_N^{4+} clusters are stable against the charge-asymmetric fission channel for $N > 74$. The most favored charged products are mostly magic clusters, Ag_N^{1+} with $N = 3, 9, 21$.

The results of charge-symmetric binary fission of Ag_N^{4+} for most favored decays are shown in Fig. 7(c). The smallest positive BH occurs at $N = 22$. The mean behavior (the dashed line) intersects the zero line at $N_2^{\text{mean}} \approx 51$.

In Fig. 7(d) we have compared the results for the three different decay processes of Ag_N^{4+} . It is seen that these clusters smaller than $N \approx 50$ are highly unstable. As is seen from the figure, it is difficult to specify the competitions for the quantal values. However, to give quantitative values, we have compared the fitted lines in Fig. 7(e). It is seen that for $N < 20$ the charge-symmetric fission is the dominant spontaneous decay process but, for $20 < N < 51$ the dominant spontaneous fission process changes to the charge-asymmetric one. For $51 < N < 73$ the only spontaneous fission decay process is the charge-asymmetric one. Clusters larger than $N_a^{\text{mean}} \approx 73$ are stable against any spontaneous decay process. In an induced fragmentation experiment of Ag_N^{4+} clusters, the dominant process for $73 < N < 107$ is charge-asymmetric fission, and for N larger than $N_c^{\text{mean}} = 107$ the evaporation process dominates. To summarize, for

smaller clusters the charge-symmetric fission is dominant, and larger clusters prefer to decay via a charge-asymmetric fission process.

Besides the most favored quantities which are strongly related to the stability of the charged cluster and were explained in the above lines, it is also interesting to calculate the DE's and BH's for a process in which the fragment products are specified. Consider the process $\text{Ag}_N^Z \rightarrow \text{Ag}_{N-1}^Z + \text{Ag}^0$ in which one of the products is a neutral monomer. We have calculated the dissociation energies $D_0^Z(N, 1)$ for all values of $Z=1, 2, 3, 4$ and $N \leq 100$. The calculated values show pronounced shell effects as in previous figures of the most favored channels. However, the mean behaviors have asymptotic constant values. For $Z = 1, 2, 3, 4$, these asymptotic values in electron-volts are 0.95, 1.00, 1.08, 1.15, respectively. This means that the monomer evaporation from a singly charged cluster needs a smaller energy than from a doubly charged and so on. The same analysis for the dimer evaporation in the process $\text{Ag}_N^Z \rightarrow \text{Ag}_{N-2}^Z + \text{Ag}_2^0$ shows also constant asymptotic mean behaviors for the $D_0^Z(N, 2)$. The obtained values in electron-volts are 0.49, 0.59, 0.72, 0.87 for $Z=1, 2, 3, 4$, respectively. This means that, as in the monomer evaporation, the detachment of a dimer from singly ionized cluster is easier than from a doubly ionized cluster and so on. However, comparing the dissociation energies for monomer and dimer evaporation (keeping the charge constant) shows that atomic evaporation needs more energy than dimer evaporation.

Now, we consider the fission processes $\text{Ag}_N^Z \rightarrow \text{Ag}_{N-2}^{Z-1} + \text{Ag}_2^{1+}$ and $\text{Ag}_N^Z \rightarrow \text{Ag}_{N-3}^{Z-1} + \text{Ag}_3^{1+}$ in which one of the fission products is a singly ionized dimer or a singly ionized trimer. The mean behaviors of the BH's for these processes are plotted in Fig. 8. As is seen, the energy needed to detach a singly ionized dimer decreases by increasing the charge of the parent cluster. This behavior should be contrasted to the behavior in the monomer or dimer evaporations. We recall that in the monomer or dimer evaporation, the dissociation energy increases by increasing the charge of the parent cluster.

It is now easy to find the mean sizes at which atomic evaporation process dominates the fission into singly ionized dimer or trimer for each charging value of the parent cluster. In doubly charged silver clusters, the monomer evaporation dominates the singly charged dimer and trimer detachments at $N = 11$ and $N = 31$, respectively. The corresponding numbers for triply charged clusters are 21 and 66. For parent clusters Ag_N^{4+} , the numbers $N = 38$ and $N = 120$ have been obtained. To summarize, by increasing the charge of the parent cluster the competition occurs at larger values of N .

IV. CONCLUSION

In this work, we have studied the fragmentations of multiply charged silver clusters taking into account the structural relaxations of the neutral and charged parent as well as daughter clusters. To calculate the relaxed-state sizes and energies of the clusters we have employed the stabilized jellium model with self-compression using a spherical geometry for the jellium background. Using these relaxed-state radius and energy for the clusters, we have calculated the dissociation energies and barrier heights for evaporation and fission processes in all possible channels. For the barrier heights, we have used the two-touching-spheres model with taking into account the polarizabilities of the two charged products. Comparison of our most favored results with the experimental data shows that our results lie under the experimental results but, the critical size for the competition of the evaporation and the fission of doubly charged silver clusters is predicted in good agreement with the experiment. This comparison also reveals that the fragmentation processes mostly occur before the complete relaxation of the charged parent clusters. That is, in the above-mentioned experiments the structural relaxation time is larger than the average time elapsed for the fragmentation of the ionized parent cluster. Having the initial (just after ionization) and the relaxed sizes $r_{s,\text{ini}}^Z, r_{s,\text{rela}}^Z$ of a Z -ply ionized cluster, one may choose an $r_{s,\text{frag}}^Z$ value ($r_{s,\text{ini}}^Z \leq r_{s,\text{frag}}^Z \leq r_{s,\text{rela}}^Z$) for the ionized cluster (just before the fragmentation) such that the calculated values coincides the experimental ones. Then using a linear interpolation it is possible to calculate the relative fragmentation time for an ionized cluster. In ordinary jellium model calculations, the assumption

$$r_s^0(N) = r_s^Z(N) = r_{s,\text{ini}}^Z(N) = r_{s,\text{frag}}^Z(N) = r_{s,\text{rela}}^Z(N) = r_{s,\text{bulk}} \quad (30)$$

is used. It should be mentioned that for exact matching of the calculated and experimental values one should use non-spherical shapes.

We have obtained the asymptotic DE's for the most favored channels in evaporation processes by fitting a simple curve on the quantal results. The result shows that the asymptotic values increase by increasing the charge of the parent cluster. In the case of Ag_N^{4+} , we have shown that for relatively small clusters the charge-symmetric fission process is dominant and then, before dominating the evaporation process the charge-asymmetric fission process overcomes. In general, the critical size (at which the evaporation dominates the fission) increases by increasing the charge of the parent cluster. The results show that the neutral p -mer dissociation energy increases by increasing the charge of the parent cluster; and for a given charged parent, the atomic evaporation needs more energy than a

dimer evaporation. Finally, it has been shown that the energy needed for the detachment of a singly charged dimer or singly charged trimer decreases by increasing the charge of the parent cluster. However, for a given parent cluster, the detachment of a singly charged trimer is easier than that of a singly charged dimer.

Acknowledgement

The author would like to thank John P. Perdew for the useful discussions and comments during this work. He also thanks Adam Kiejna for providing me with his recent review article on the stabilized jellium model.

-
- ¹ U. Näher, S. Bjørnholm, S. Frauendorf, F. Garcias, and C. Guet, Phys. Rep. **285**, 245 (1997) and references therein.
- ² C. Yannouleas, U. Landman, and R. N. Barnett, *Metal Clusters*, edited by W. Ekardt (Wiley, New York, 1999) pp. 145-180.
- ³ W. E. Ekardt, Phys. Rev. B **29**, 1558 (1984).
- ⁴ W. D. Knight, K. Clemenger, W. A. de Heer, W. A. Saunders, M. Y. Chou, and M. L. Cohen, Phys. Rev. Lett. **52**, 2141 (1984).
- ⁵ M. Brack, Rev. Mod. Phys. **65**, 677 (1993), and references therein.
- ⁶ H. A. Jahn and E. Teller, Proc. R. Soc. London, Ser. A **161**, 220 (1937).
- ⁷ J. P. Perdew, H. Q. Tran, and E. D. Smith, Phys. Rev. B **42**, 11627 (1990).
- ⁸ H. B. Shore and J. H. Rose, Phys. Rev. B **59**, 10485 (1999) and references therein.
- ⁹ N. D. Lang and W. Kohn, Phys. Rev. B **1**, 4555 (1970).
- ¹⁰ N. W. Ashcroft and D. C. Langreth, Phys. Rev. **155**, 682 (1967).
- ¹¹ A. B. Alchagirov, J. P. Perdew, J. C. Boettger, R. C. Albers, and C. Fiolhais, Phys. Rev. B **63**, 224115 (2001).
- ¹² C. Fiolhais and J. P. Perdew, Phys. Rev. B **45**, 6207 (1992).
- ¹³ A. Kiejna, Prog. Surf. Sci. **61**, 85 (1999).
- ¹⁴ I. Sarria, C. Henriques, C. Fiolhais, and J. M. Pitarke, Phys. Rev. B **62**, 1699 (2000).
- ¹⁵ J. P. Perdew, M. Braczkewska, and C. Fiolhais, Solid State Commun. **88**, 795 (1993).
- ¹⁶ M. Seidl, J. P. Perdew, M. Braczkewska, and C. Fiolhais, J. Chem. Phys. **108**, 8182 (1998).
- ¹⁷ M. Payami, J. Phys.: Condens. Matter **13**, 4129 (2001).
- ¹⁸ P. Ziesche, M. J. Puska, T. Korhonen, and R. M. Nieminen, J. Phys.: Condens. Matter **5**, 9049 (1993).
- ¹⁹ A. Vieira, M. Braczkewska, and C. Fiolhais, Int. J. Quantum Chem. **56**, 239 (1995).
- ²⁰ A. Vieira and C. Fiolhais, Phys. Rev. B **57**, 7352 (1998).
- ²¹ M. Braczkewska, A. Vieira, C. Fiolhais, and J. P. Perdew, Prog. Surf. Sci. **53**, 305 (1996).
- ²² A. Kiejna and V. V. Pogosov, J. Phys.: Condens. Matter **8**, 4245 (1996).
- ²³ M. Payami, J. Chem. Phys. **111**, 8344 (1999).
- ²⁴ W. Kohn and L. J. Sham, Phys. Rev. **140**, A1133 (1965).
- ²⁵ P. Hohenberg and W. Kohn, Phys. Rev. B **136**, 864 (1964).
- ²⁶ M. Payami and N. Nafari, J. Chem. Phys. **109**, 5730 (1998).
- ²⁷ J. P. Perdew and Y. Wang, Phys. Rev. B **45**, 13244 (1992).
- ²⁸ N. W. Ashcroft, Phys. Lett. **23**, 48 (1966).
- ²⁹ C. J. F. Böttcher, *Theory of Electric Polarization* (Elsevier, Amsterdam, 1973).
- ³⁰ S. Krückeberg, G. Dietrich, K. Lützenkirchen, L. Schweikhard, and J. Ziegler, Phys. Rev. A **60**, 1251 (1999).
- ³¹ U. Kreibig and M. Vollmer, *Optical Properties of Metal Clusters* (Springer, 1995).
- ³² M. Nakamura, Phys. Rev. A **60**, 2222 (1999).
- ³³ H. Koizumi, S. Sugano, and Y. Ishii, Z. Phys. D **26**, 264 (1993).
- ³⁴ H. Koizumi, S. Sugano, and Y. Ishii, Z. Phys. D **28**, 223 (1993).
- ³⁵ S. Krückeberg, G. Dietrich, K. Lützenkirchen, L. Schweikhard, C. Walther, and J. Ziegler, J. Chem. Phys. **110**, 7216 (1999).
- ³⁶ I. Katakuse, H. Itoh, and T. Ichihara, Int. J. Mass Spectrom. Ion Processes **97**, 47 (1990).

FIG. 1. Fission barrier in the two-touching-spheres model. B , D , and E_c are barrier height, dissociation energy, and the coulomb energy between two touching charged conductors, respectively.

FIG. 2. The equilibrium r_s values in atomic units for Z -charged clusters as a function of the cluster size N . The dashed line is the bulk Wigner-Seitz radius for Ag ($r_s = 3.02$).

FIG. 3. The equilibrium total energies per atom in electron volts for Z -charged clusters as a function of the cluster size N . The dashed line is the bulk SJM value for Ag ($\epsilon = -7.89\text{eV}$).

FIG. 4. (a)- The right vertical axis shows the size of the fragment in the most favored channel, p^* , of singly ionized clusters by small solid squares. The left vertical axis shows the dissociation energies, DE, in electron volts for the most favored decay channels of singly ionized clusters by large open square symbols. The dashed line is the fitting result which has the asymptotic value of 0.20eV . (b)- The dissociation energies for monomer ($p = 1$), dimer ($p = 2$), and the most favored ($p = p^*$) p^* -mers are compared with the experiment. The figures on the experimental data points specify the fragment size p . The experiment shows an odd-even staggering.

FIG. 5. (a)- The same as in Fig. 4(a) for doubly ionized clusters, with the asymptotic value of the dashed fitted line as 0.40eV . (b)- The most favored size of the fragments, p^* , and the barrier heights for this most favored values in electron volts as function of the cluster size N . The dashed fitted line intersects the zero axis at $N = 29$. (c)- Comparison of the most favored values of the DE's and the BH's. $E_{z_1}^{2+}$ is D_0^{2+} for $z_1 = 0$ and B_{1+}^{2+} for $z_1 = 1$. Evaporation starts from $N = 21$. (d)- Comparison of the most favored DE's and BH's with the experiment. The figures on the experimental data points show the fragment sizes. (e)- Comparison of the monomer DE's and the singly ionized trimer BH's with the experiment.

FIG. 6. (a)- The same as in Fig. 4(a) for triply ionized clusters, with the asymptotic value of the dashed fitted line as 0.50eV . (b)- The same as in Fig. 5(b) with the intersection point at $N = 53$. (c)- The same as in Fig. 5(c) with starting the evaporation from $N = 38$.

FIG. 7. (a)- The same as in Fig. 4(a) for 4-ply ionized clusters, with the asymptotic value of the dashed fitted line as 0.75eV . (b)- The same as in Fig. 5(b) for charge-asymmetric fission with the intersection point at $N_1 = 74$. (c)- The same as in Fig. 5(b) for charge-symmetric fission with the intersection point at $N_2 = 51$. (d)- Comparison of the evaporation DE's with the charge-asymmetric ($z_1 = 1$) and the charge-symmetric ($z_1 = 2$) fission BH's. (e)- Comparison of the fitted lines for the processes in (d). At $N = 20$, the charge-symmetric and the charge-asymmetric fissions compete. For $N > 51$, charge-symmetric and for $N > 73$, the charge-asymmetric fissions stop, respectively. For $N_c^{\text{mean}} > 107$ evaporation overcomes the fission processes.

FIG. 8. Comparison of the fitted values of the BH's for dissociating a singly ionized dimer or trimer from a Z -ply charged cluster.

Fig. 1, M. Payami

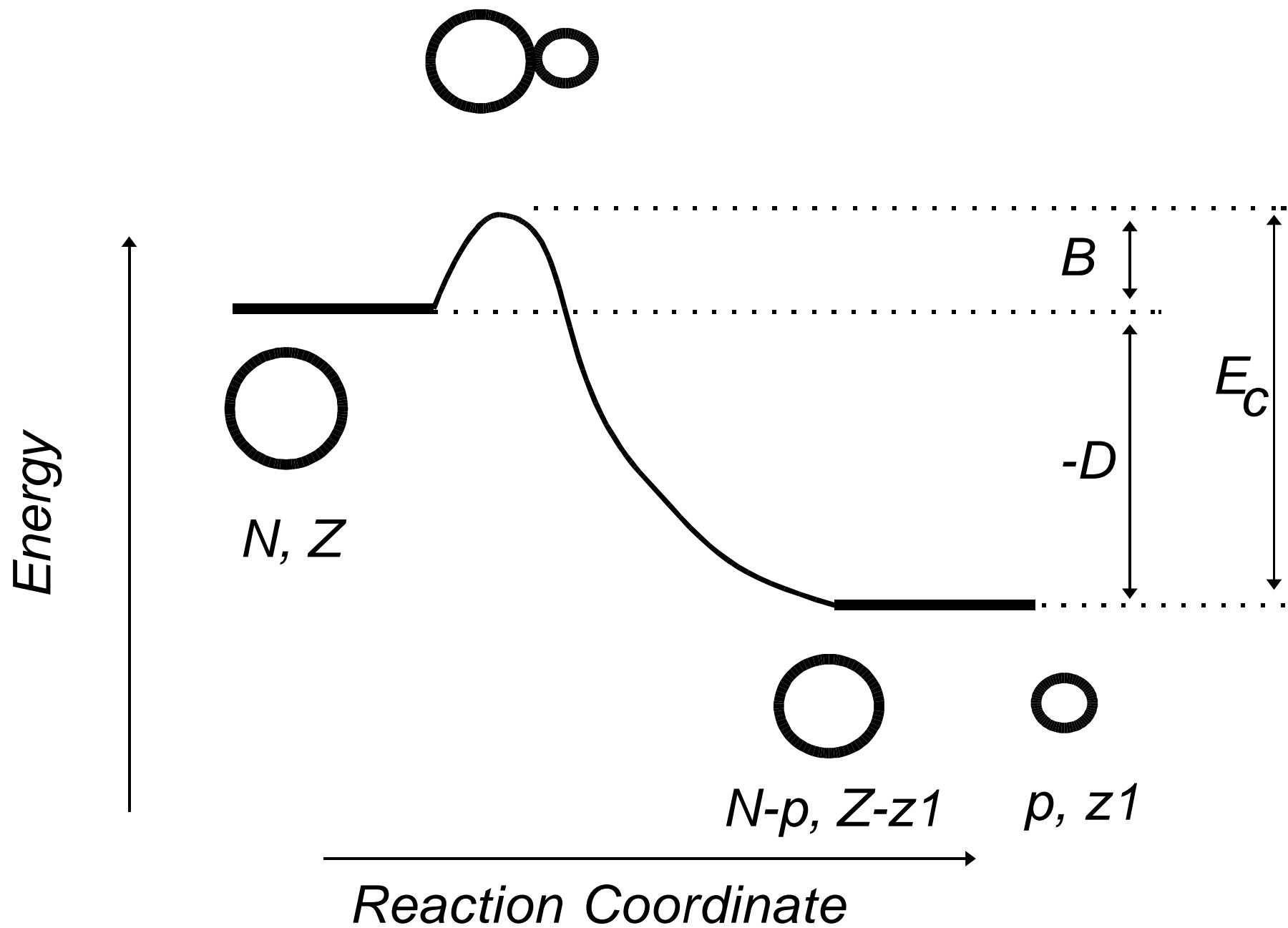


Fig. 2, M. Payami

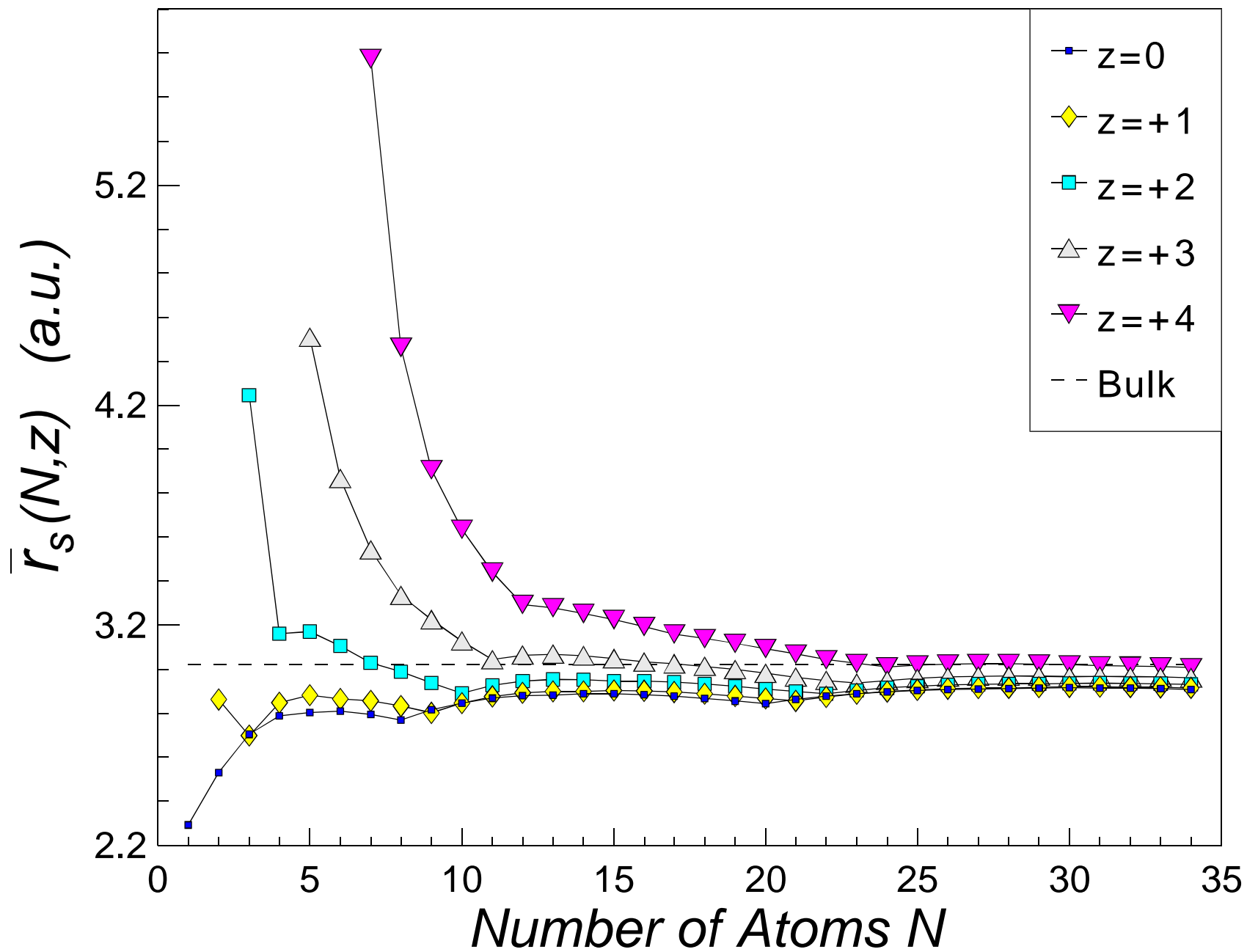


Fig. 3, M. Payami

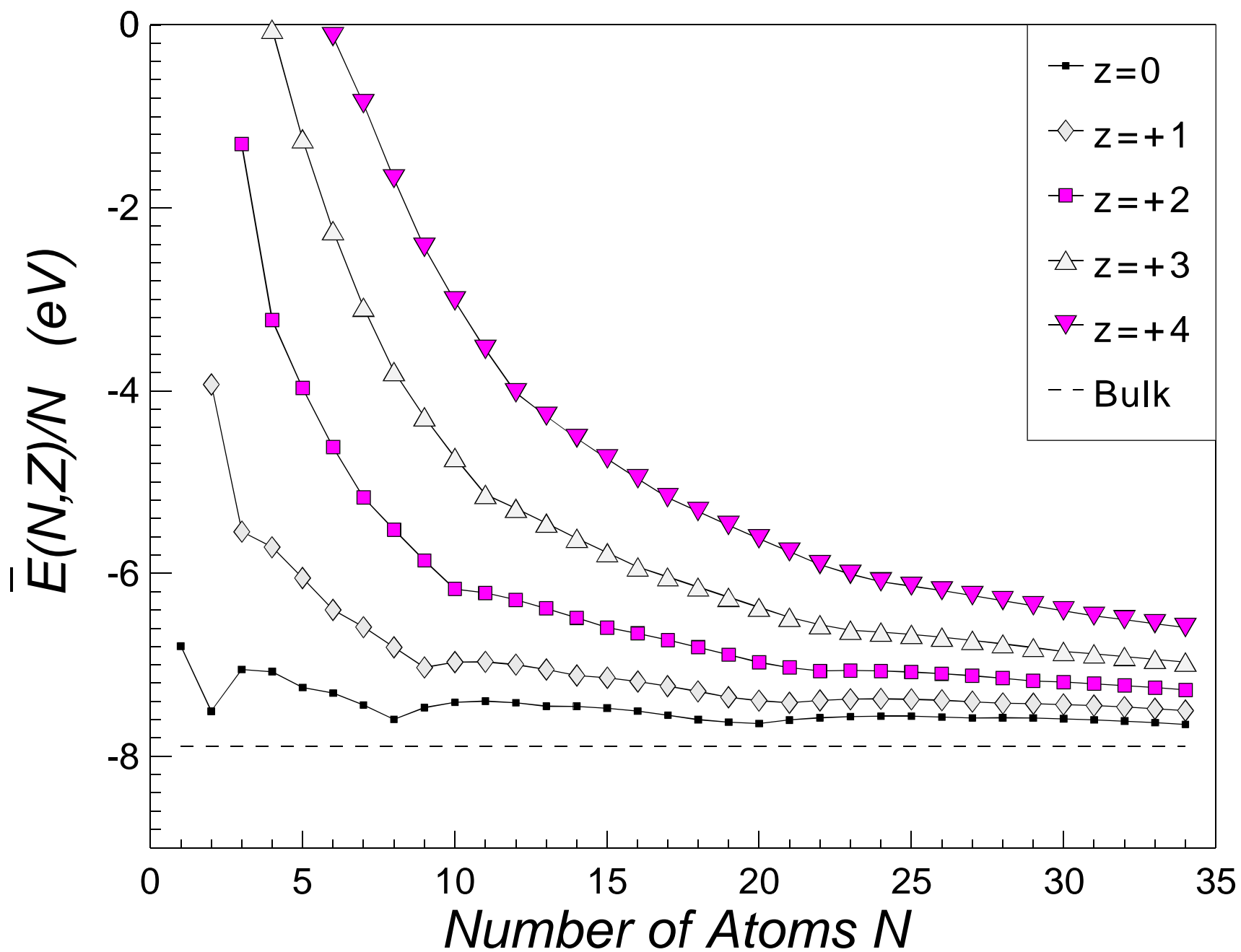


Fig. 4(a), M. Payami

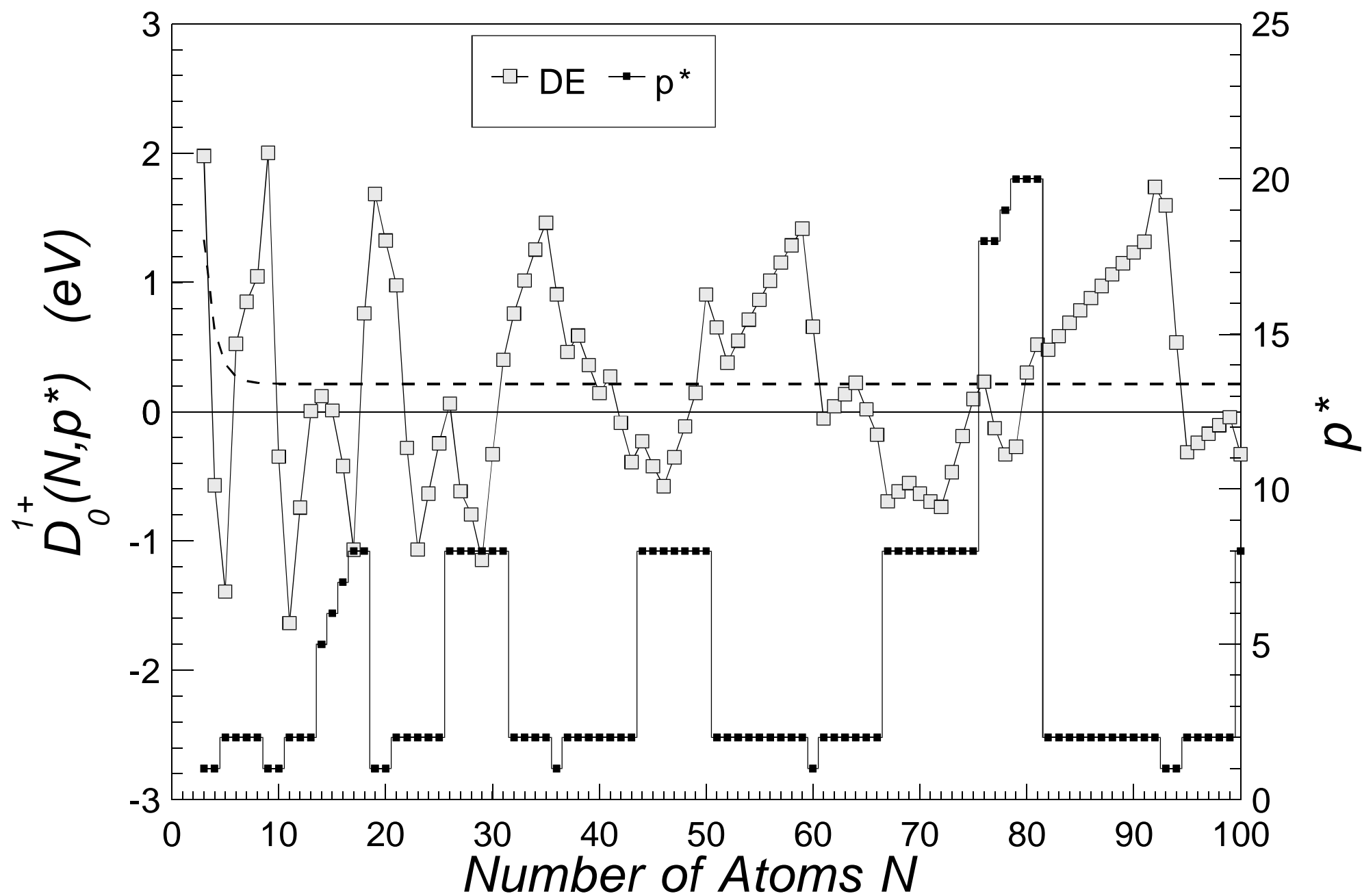


Fig. 4(b), M. Payami

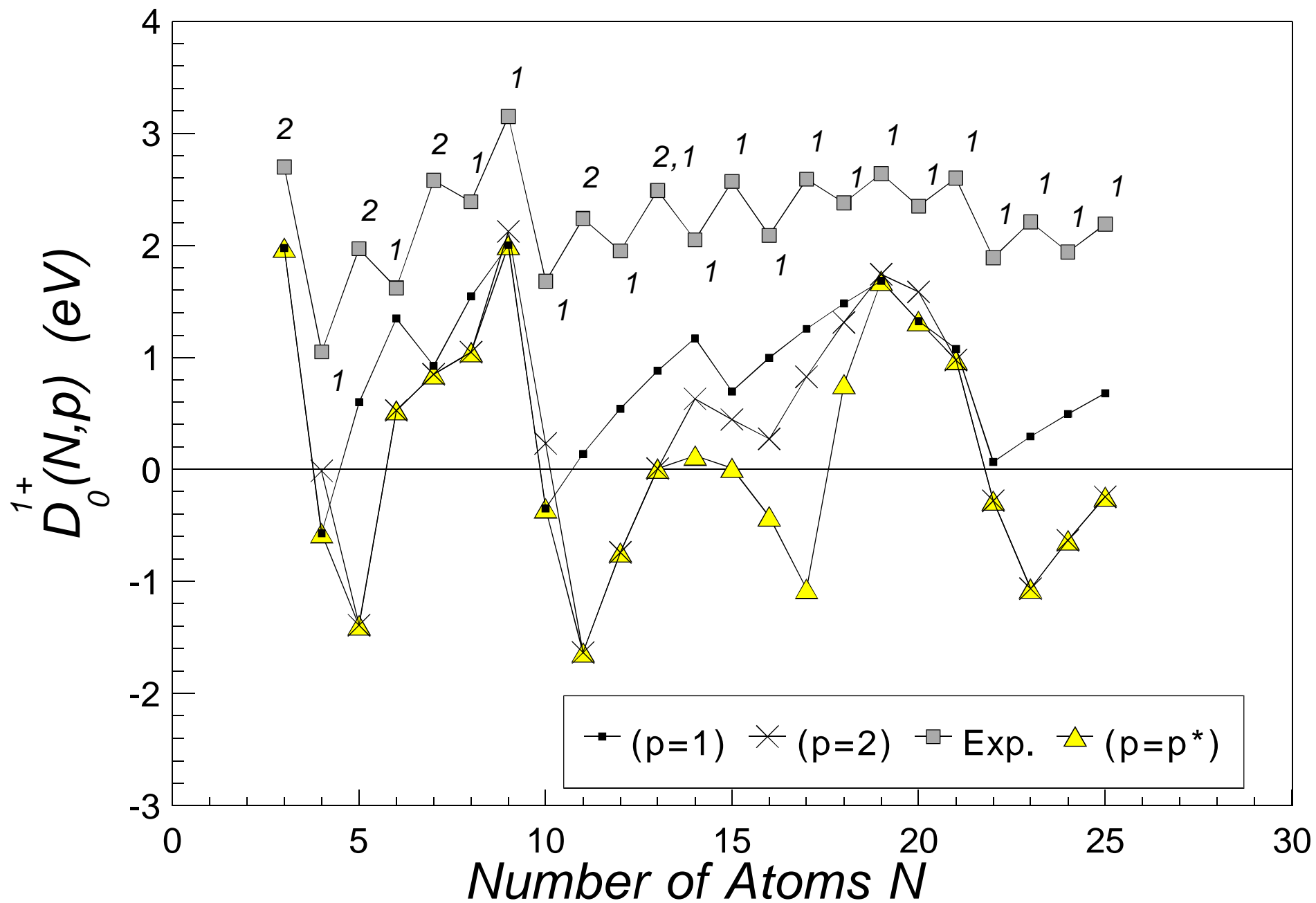


Fig. 5(a), M. Payami

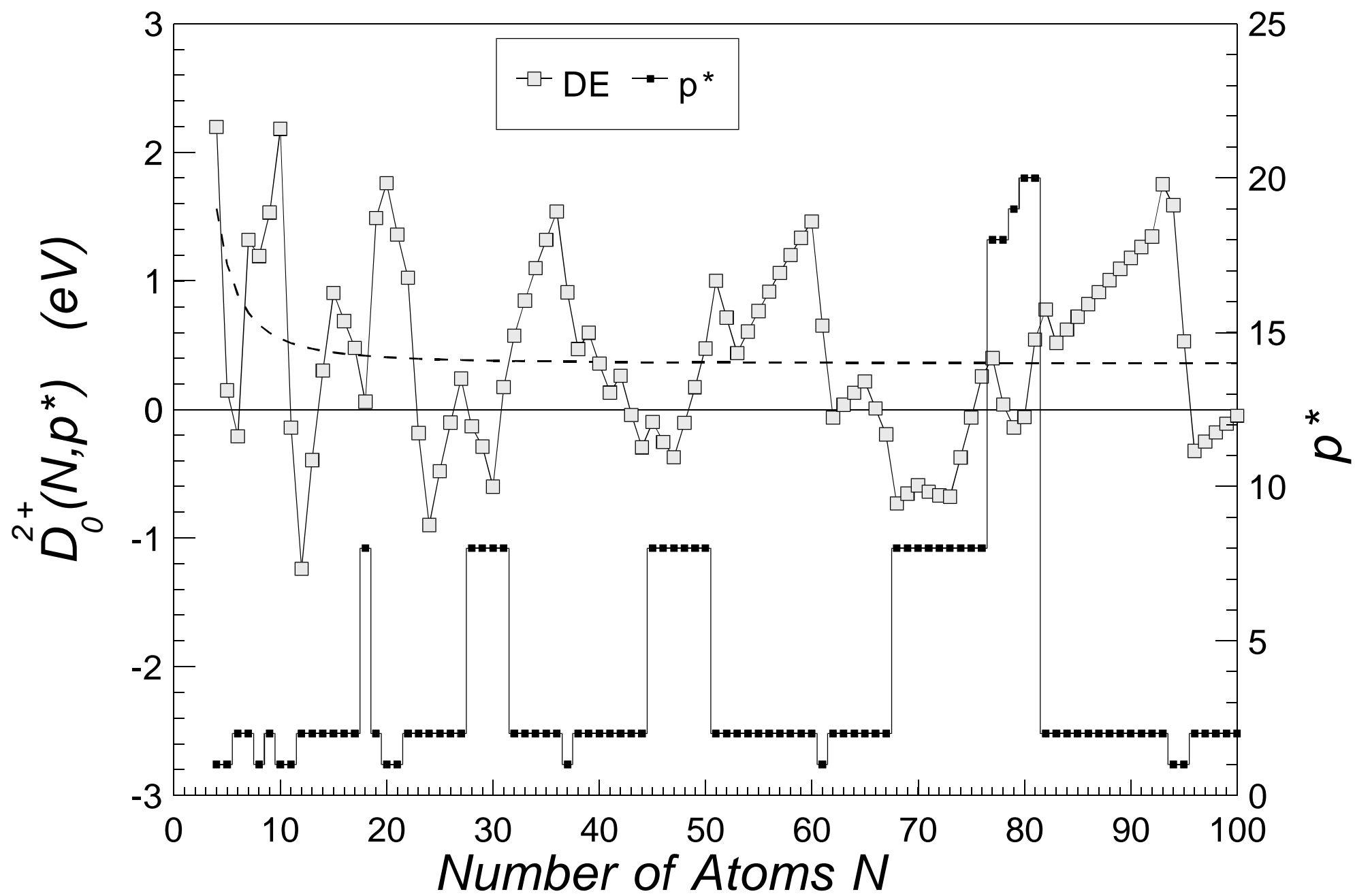


Fig. 5(b), M. Payami

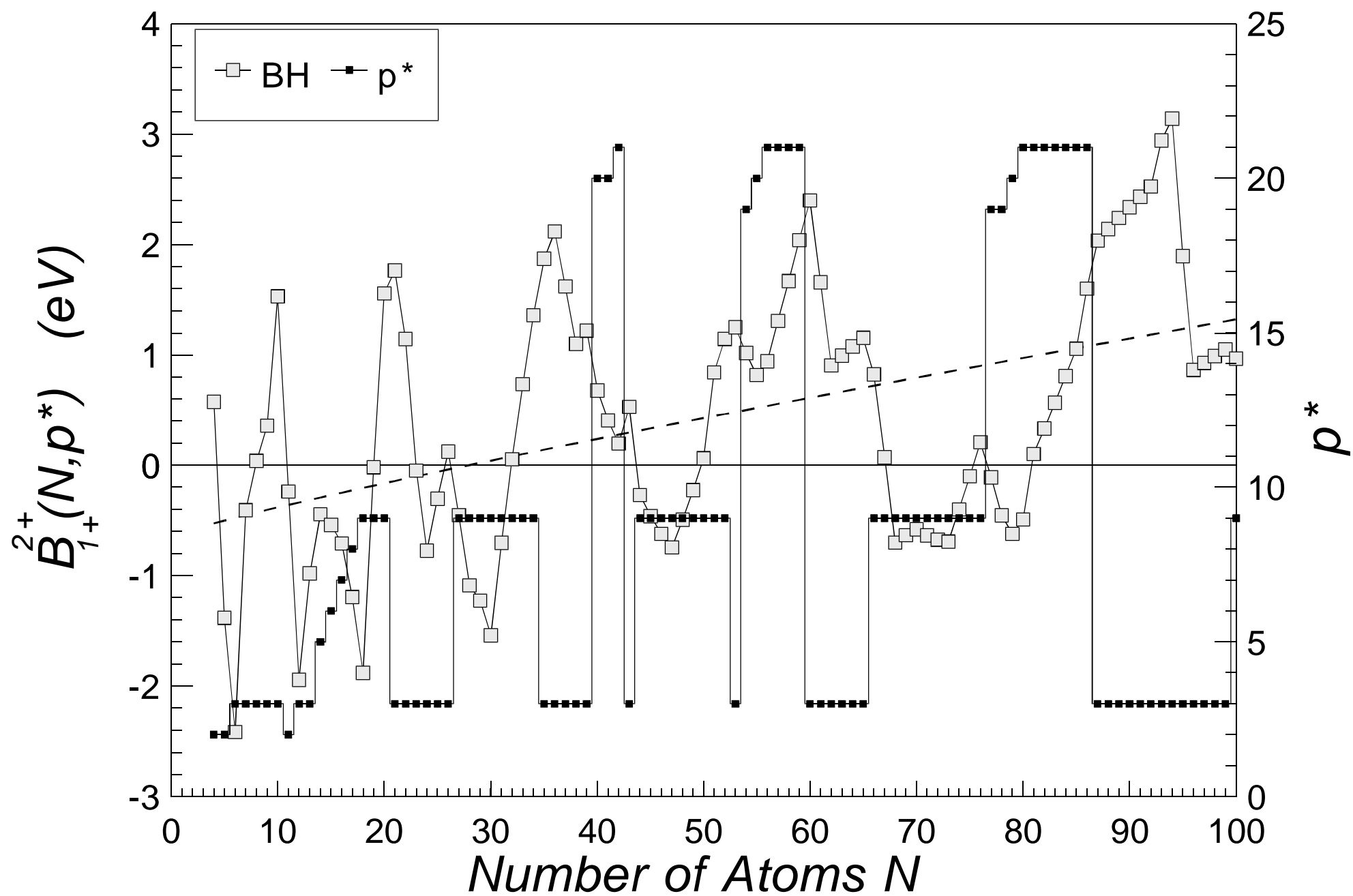


Fig. 5(c), M. Payami

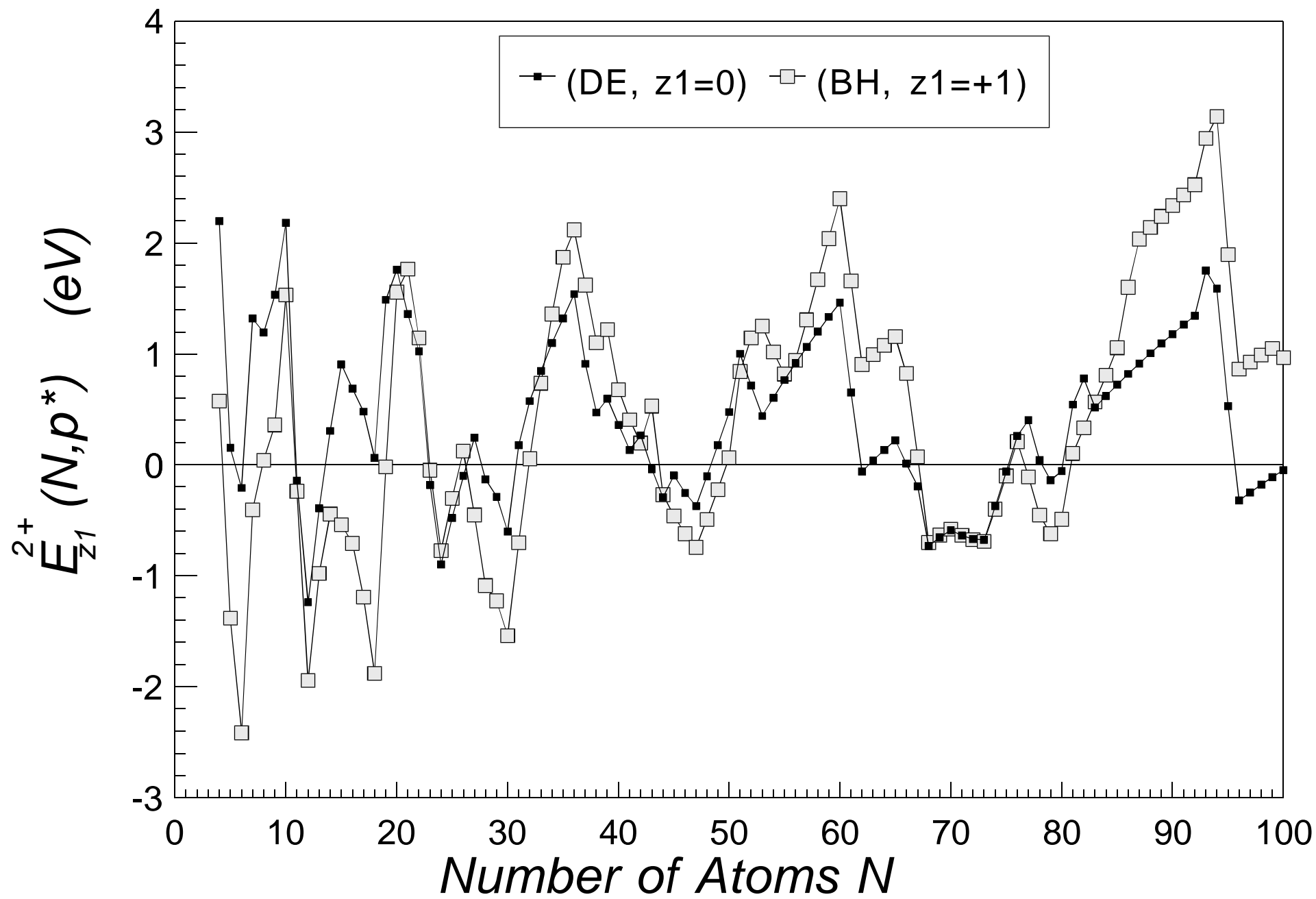


Fig. 5(d), M. Payami

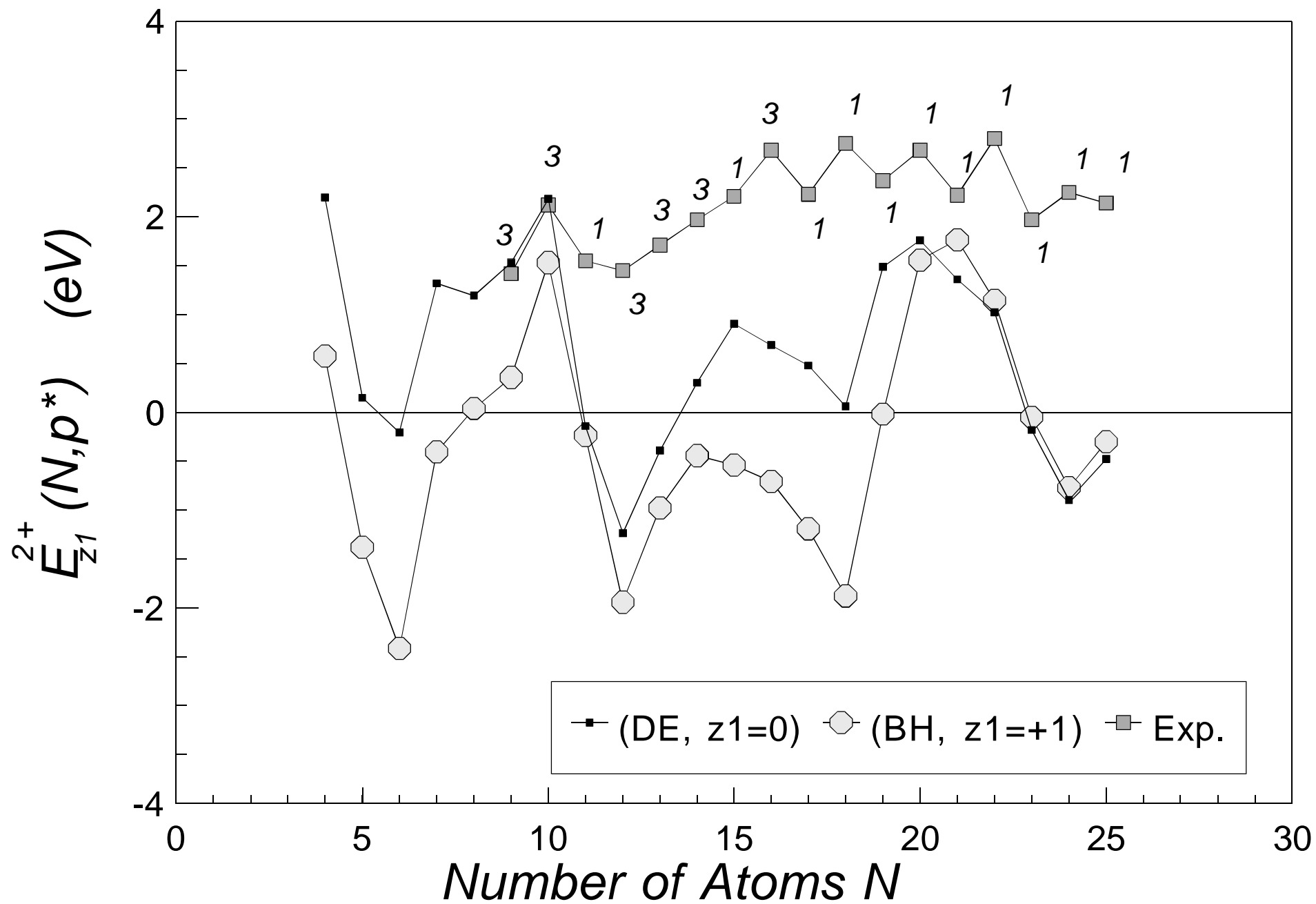


Fig. 5(e), M. Payami

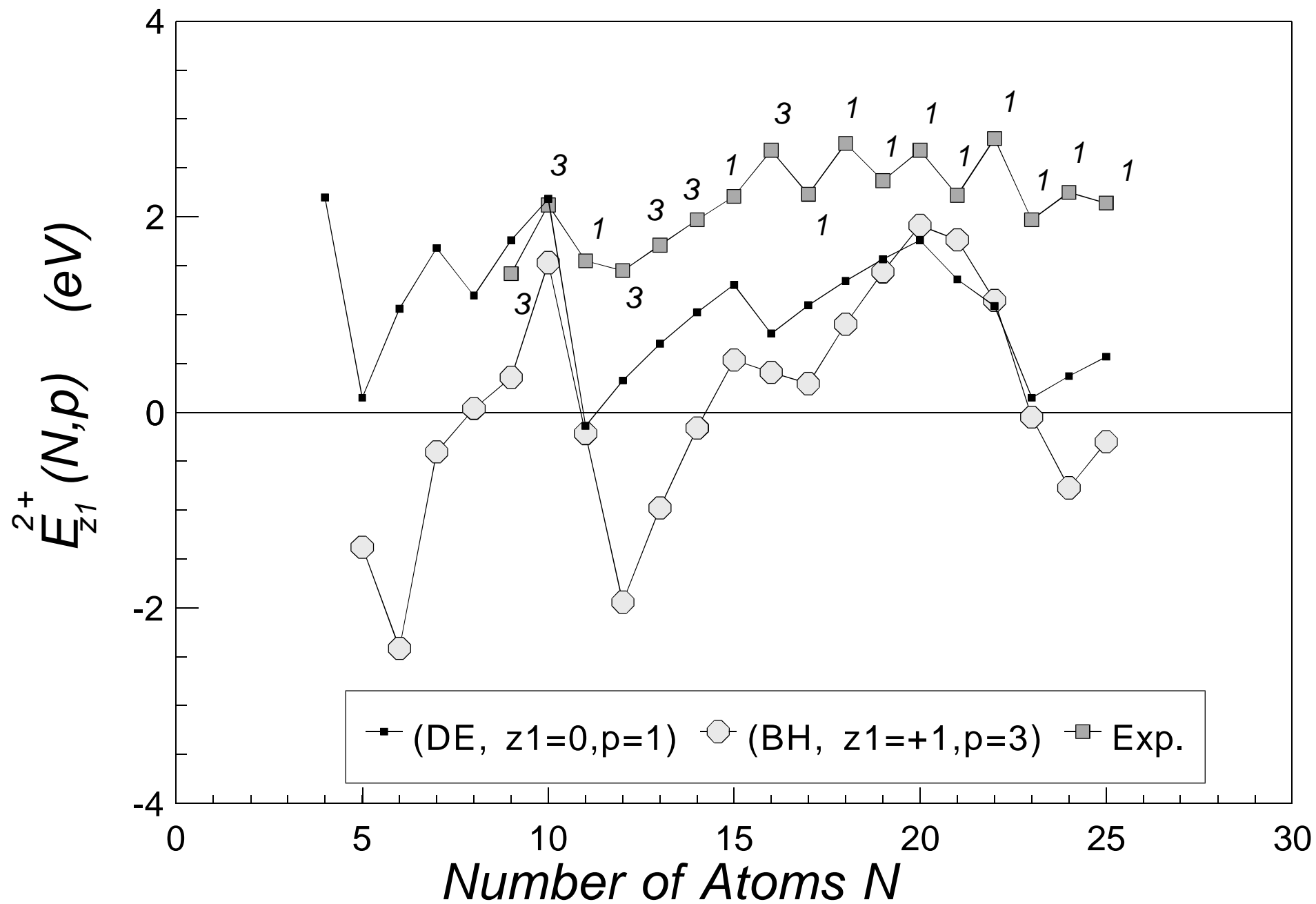


Fig. 6(a), M. Payami

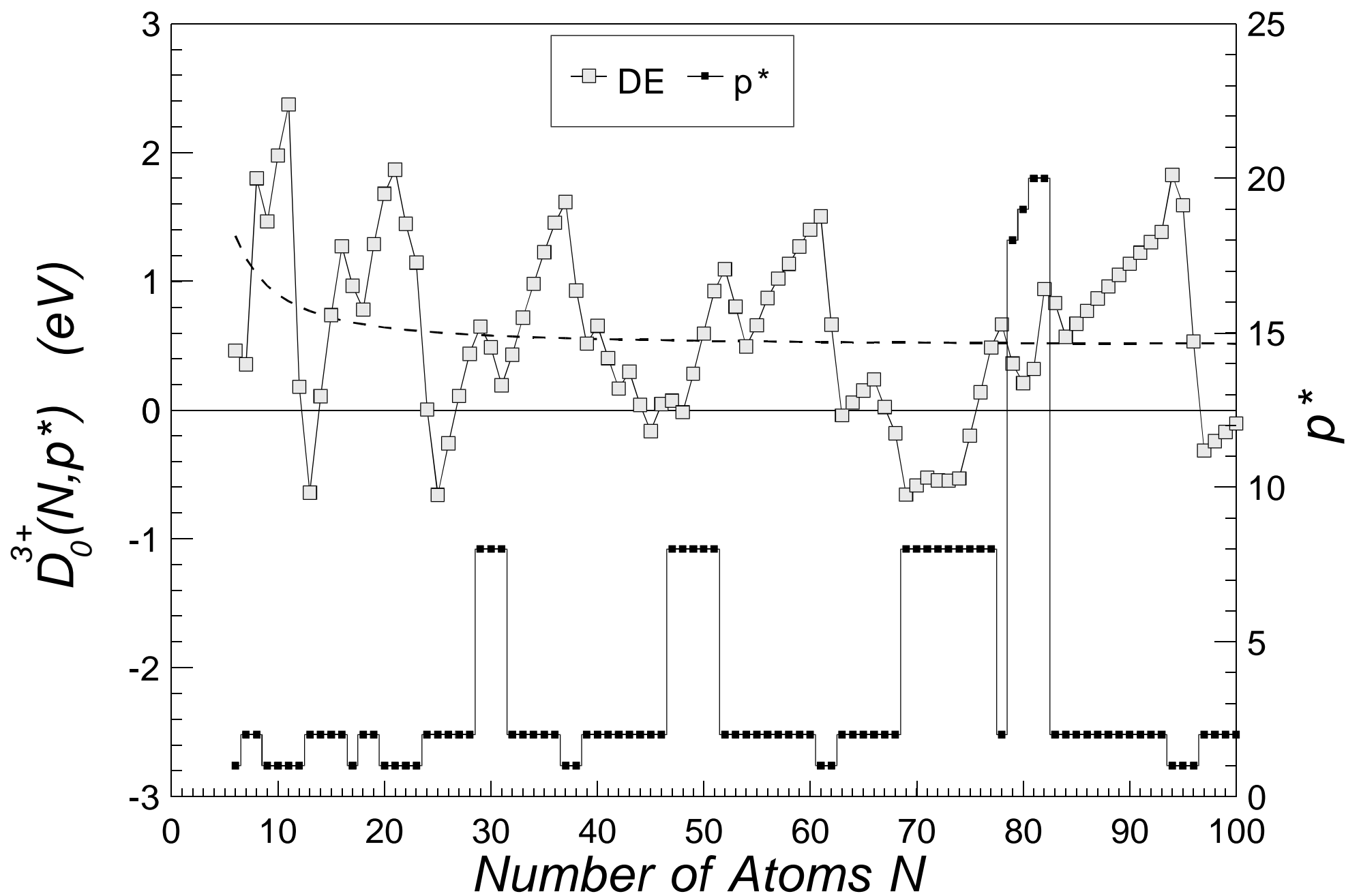


Fig. 6(b), M. Payami

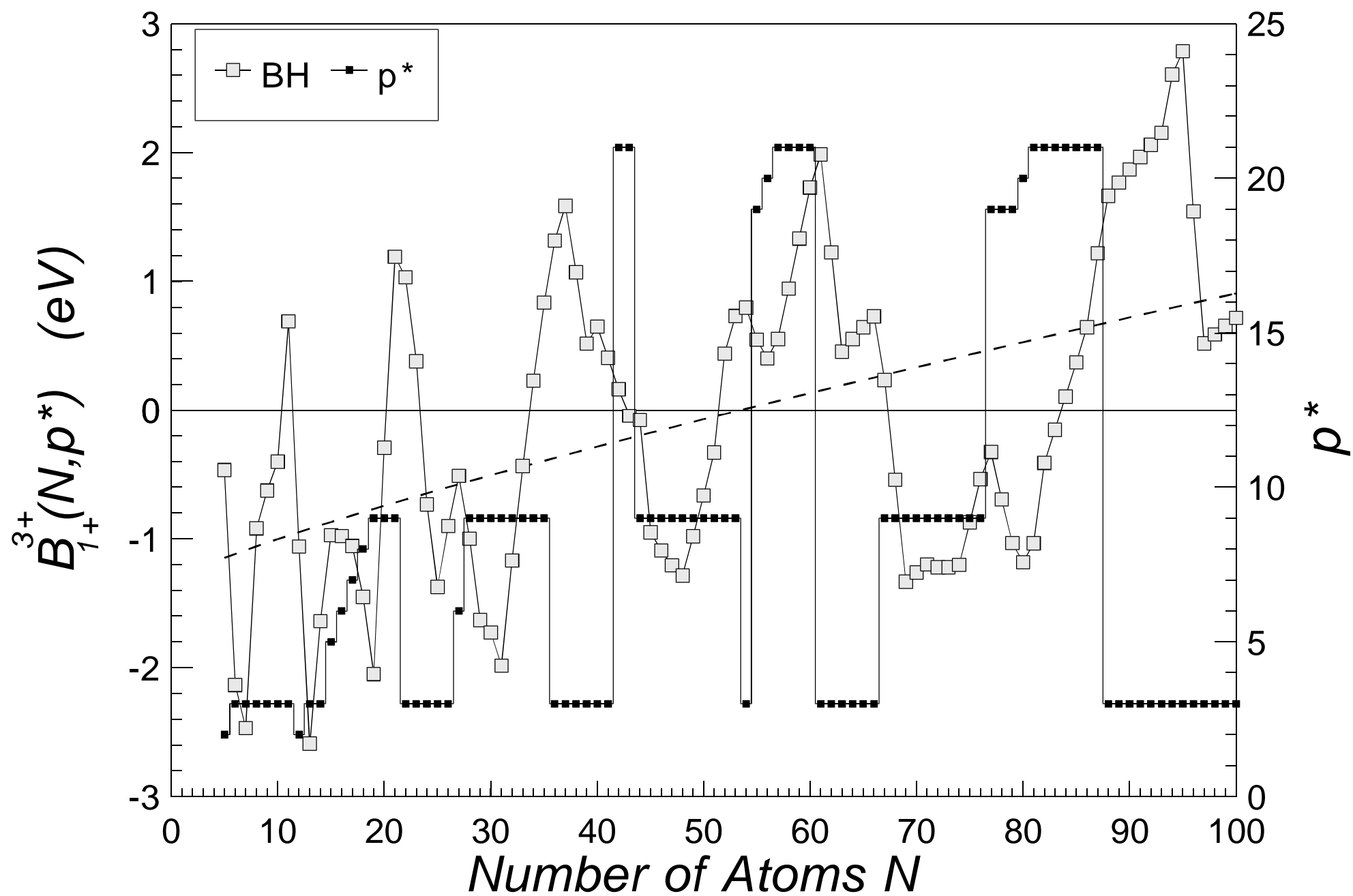


Fig. 6(c), M. Payami

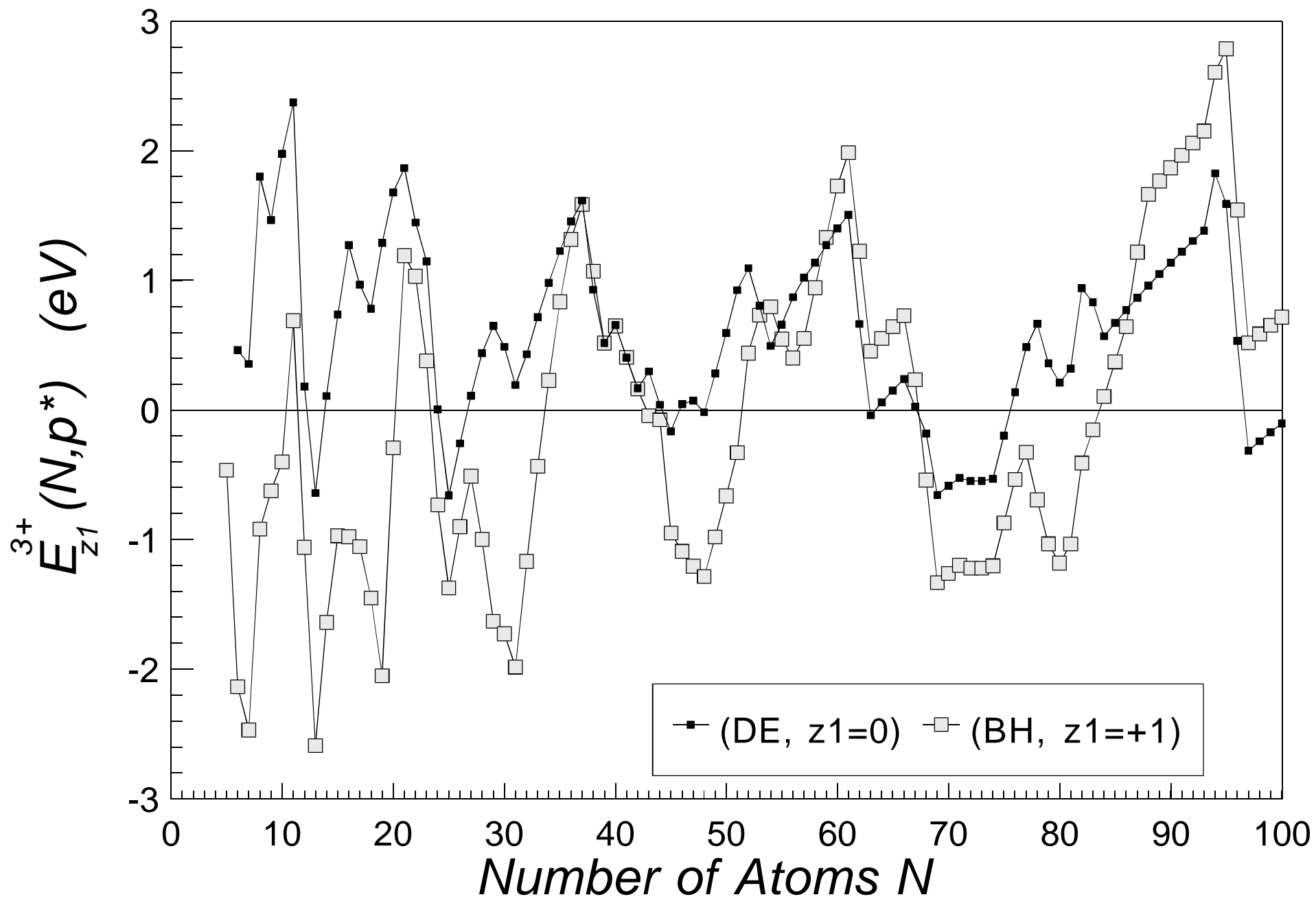


Fig. 7(a), M. Payami

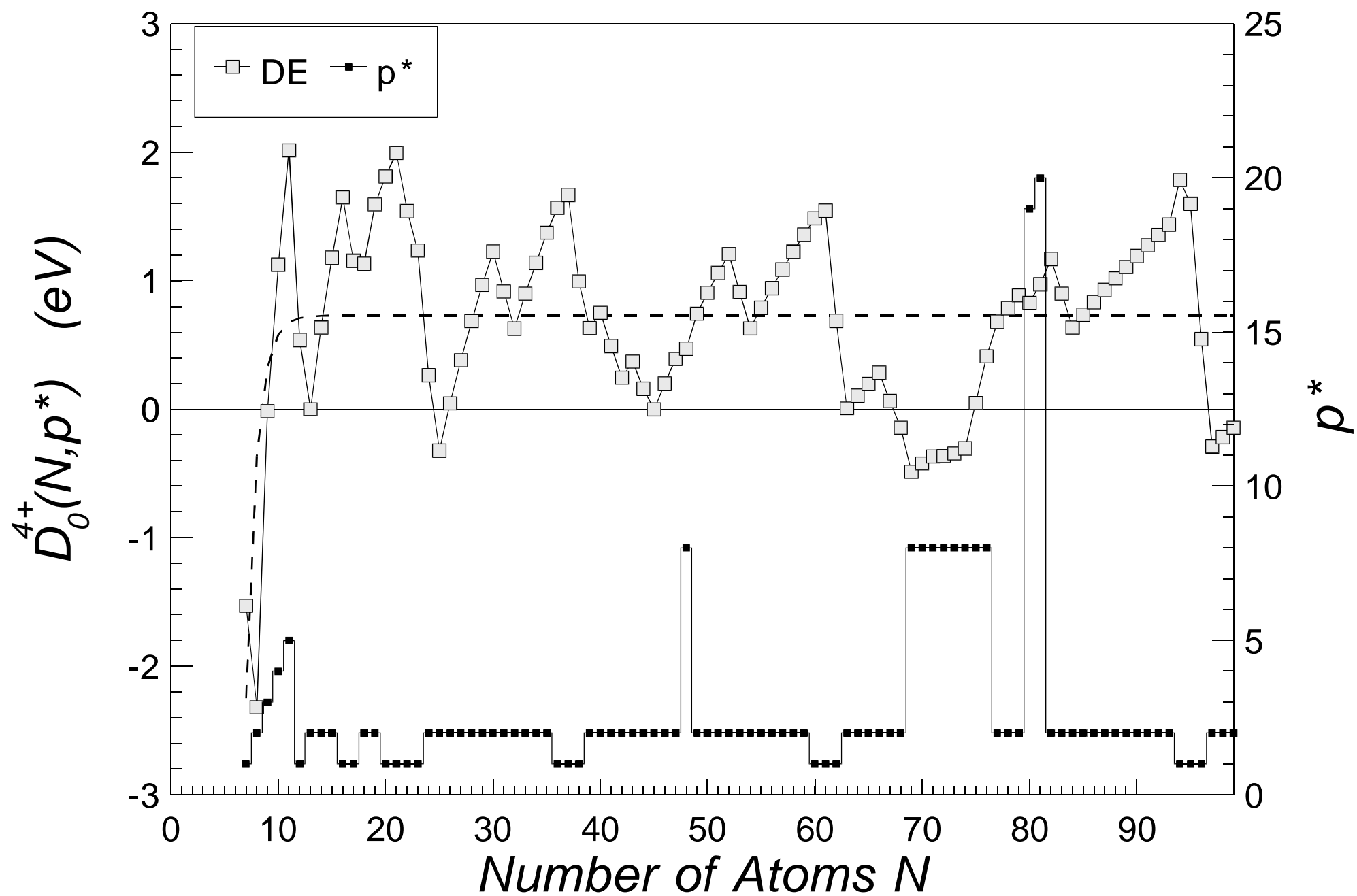


Fig. 7(b), M. Payami

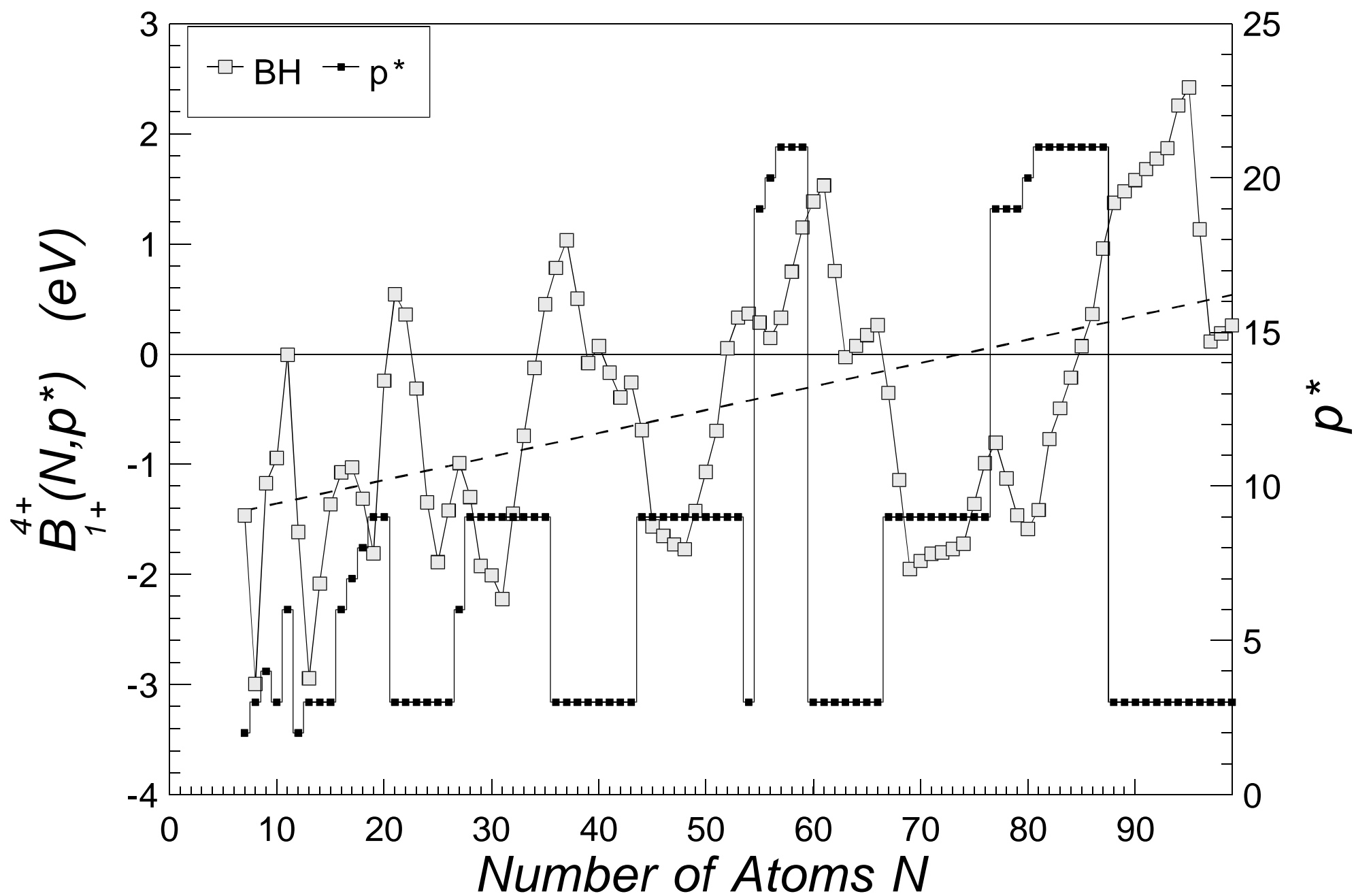


Fig. 7(c), M. Payami

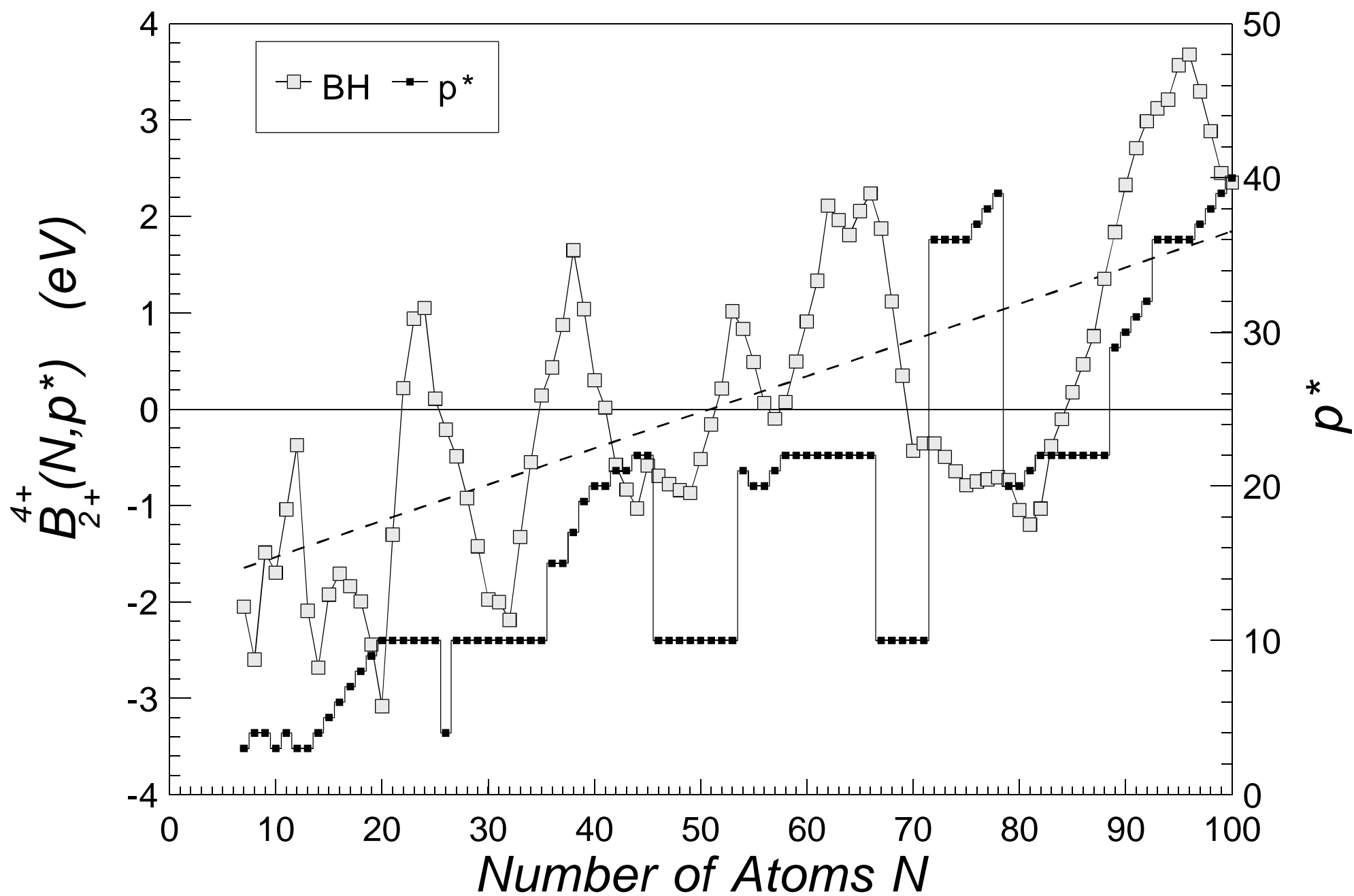


Fig. 7(d), M. Payami

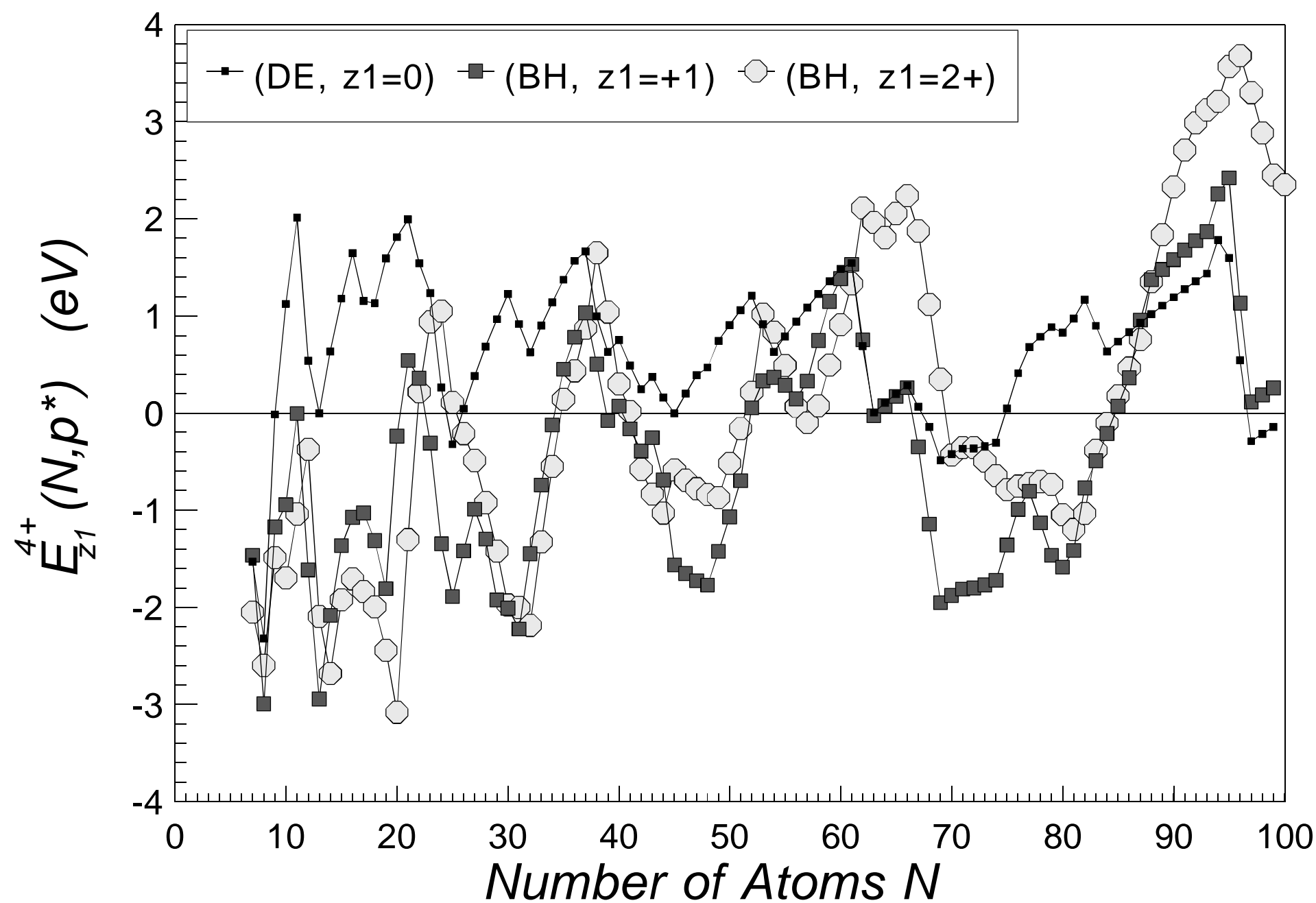


Fig. 7(e), M. Payami

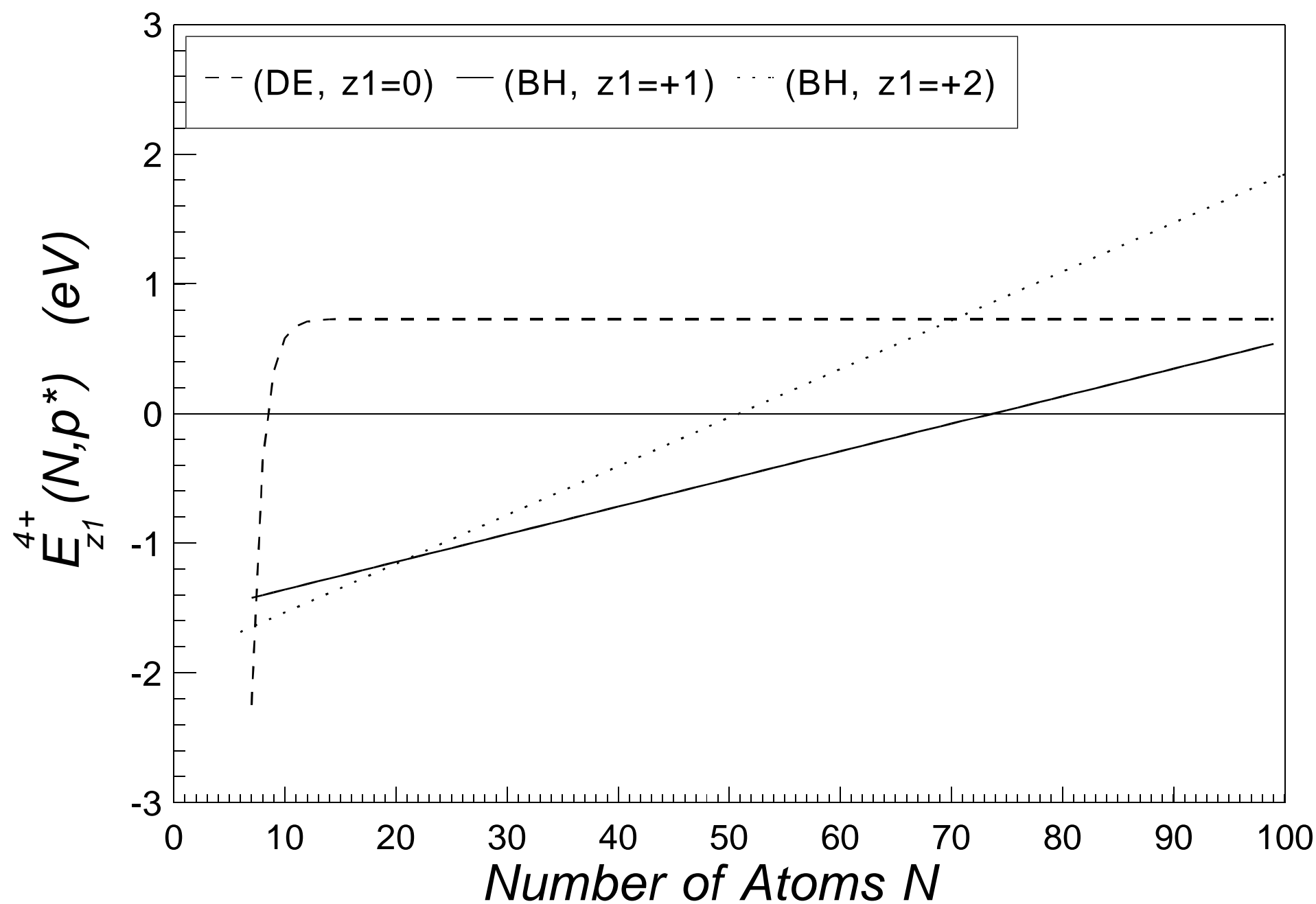


Fig. 8, M. Payami

